UNIVERSIDADE
BEIRA INTERIOR

# Design and Characterization of an Adhesive for T-Joint Composite

(Versão final após defesa)

**Hugo Micael Santos Valente**

Dissertação para obtenção do Grau de Mestre em

**Engenharia Aeronáutica**

(Mestrado integrado)

Orientador: Prof. Doutor Abílio Manuel Pereira da Silva

**agosto de 2020**

This page was left intentionally blank

# Acknowledgments

First, I would like to offer my sincerest and deepest gratitude to Prof. Abílio Silva whose expertise and support throughout all the work done was invaluable.
To Prof. Paulo N.B. Reis, for discussing the results and proposals for the work.
To Eng. João Cardoso and Eng. Paulo Santos, whose experience and outstanding support helped me throughout all the work developed.
To Department of Aerospace Sciences and Department of Electromechanical Engineering for the availability of the facilities.
To C-MAST - Center for Aerospace Sciences and Technologies (www.aerospace.ubi.pt; FCT unit #151) for providing the materials for this work.
To my family, especially my father and godmother for providing me with all the conditions and support to finish the degree that I love.
To all by friends for making the good moments great and the bad moments bearable.

This Master Dissertation has been supported by the project Centro-01-0145-FEDER-000017 - EMaDeS - Energy, Materials and Sustainable Development, co-financed by the Portugal 2020 Program (PT 2020), within the Regional Operational Program of the Center (CENTRO 2020) and the European Union through the European Regional Development Fund (ERDF).

Cofinanciado por:

# Resumo

Com o aumento do uso de compósitos em estruturas aeronáuticas, em particular matrizes poliméricas reforçadas com fibras de carbono (CFRP), também aumenta o uso de diversos tipos de juntas, sendo uma das mais comuns as juntas em T. O sistema de união com maior interesse são os adesivos estruturais, mas a otimização do seu uso requer a compreensão do seu comportamento em diferentes condições de solicitação.
Neste trabalho, o adesivo estrutural aeronáutico na forma de filme SEAL® EA451 U150, foi caracterizado à flexão em 3 pontos usando diferentes velocidades de ensaio, à relaxação de tensões e à fluência. O adesivo foi exposto a temperaturas de 20ºC, 40ºC e 80ºC, imerso em água e a degradação das propriedades mecânicas (estáticas e viscoelásticas) foram avaliadas. Finalmente, este adesivo foi usado em juntas em T e foram realizados ensaios de arrancamento (SPOT) por forma a compreender o efeito da exposição à temperatura e humidade nos mecanismos de ruína dominantes.
Os resultados mostram que: as propriedades mecânicas em flexão em 3 pontos do adesivo dependem das condições de solicitação: -observou-se que a resistência mecânica (tensão) e o módulo de elasticidade aumentam com a velocidade de ensaio; -para uma carga de 60 % da tensão de rutura após 180 minutos a redução de carga é inferior a 10 %. Após a degradação ambiental verifica-se que o adesivo perde resistência (de 109 para 62 N) e diminui a deformação (de 3,4 para 1,8 %). As juntas em T nos ensaios SPOT têm um mecanismo de ruína progressivo (não abrupto) e quando sujeitas a degradação ambiental apresentam uma redução na carga máxima de ~8 %, mas um aumento na deformação de ~18 %.

# Palavras-chave

CFRP; adesivo estrutural; propriedades mecânicas; degradação ambiental; ensaios de arrancamento; juntas em T; modo de falha.

This page was left intentionally blank

# Abstract

With the increase in composites usage in aeronautical structures and with it, the use of Carbon-Fiber Reinforced Polymers (CFRP), there was also an increase in the use of diverse types of joints, being one of the most common the T-joints. The bonding method that has gained a lot of attention is the adhesive bonding, but its optimization requires an understanding of its behavior with different types of service conditions.
In this work, the aeronautical structural adhesive film SEAL® EA451 U150 was characterized at 3-point bending using different strain-rates, stress relaxation and creep behavior. The adhesive was subjected to different temperatures while immersed in water and the degradation of properties (mechanical and viscoelastic) were evaluated. Finally, this adhesive was used in T-joints and Stiffener Pull-Off Tests (SPOT) were conducted in order to understand the effect of exposure to temperature and moisture on the failure mode.
The results show that: the mechanical properties in 3-point bending of the adhesive depend on the service conditions: -it was observed that the ultimate stress strength and the elastic modulus increase with the strain-rate; - for a load of 60 % of the ultimate stress strength after 180 minutes the stress decrease is inferior to 10 %. After suffering environmental degradation, the adhesive decreases its ultimate stress strength (from 109 to 62 N) and decreases its maximum strain (from 3.4 to 1.8 %), T-joints in SPOT have a progressive failure mode (non-abrupt) and when subjected to environmental degradation present a reduction of maximum load of ~8%, but with an increase of ~18 % in deformation.

# Keywords

CFRP, structural adhesive, mechanical properties, environmental degradation, SPOT, T-joints, failure mode.

This page was left intentionally blank

# Table of Contents

# List of Figures

# List of Tables

This page was left intentionally blank

# List of Acronyms

| | |
|---|---|
| ASTM | American Society for Testing and Materials |
| CFRP | Carbon Fiber-Reinforced Polymer |
| FEM | Finite Element |
| FRP | Fiber-Reinforced Polymer |
| IMCs | Intermetallic compounds |
| SHM | Structural Health Monitoring |
| SPOT | Stiffener Pull-Off Test |
| TDS | Technical Datasheet |
| UD | Unidirectional |
| USS | Ultimate stress strength |
| UV | Ultraviolet |

This page was left intentionally blank

# List of Symbols

| | | |
|---|---|---|
| A | [mm/s] | amplitude of transient creep |
| B | [g/cm$^3$] | bulk density |
| b | [mm] | width of specimen |
| d | [mm] | depth of specimen |
| D | [mm] | deflection on center of the beam |
| $D_f$ | [GPa$^{-1}$] | Creep Compliance Function |
| $D_w$ | [g] | dry weight |
| E | [GPa] | modulus of elasticity |
| $E_B$ | [MPa] | modulus of elasticity in bending |
| L | [mm] | support span |
| m | [N/mm] | slope of tangent of the load-deflection curve |
| n | | constant independent of stress |
| $P_a$ | [%] | apparent porosity |
| $P_l$ | [N] | load applied |
| $P_{max}$ | [N] | maximum load applied |
| S | [g] | suspended weight |
| V | [cm$^3$] | exterior volume |
| W | [g] | saturated weight |
| $\beta$ | | fractional power exponent |
| $\delta$ | [mm] | displacement |
| $\delta_{Pmax}$ | [mm] | displacement for maximum load applied |
| $\delta_{max}$ | [mm] | maximum displacement |
| $\varepsilon$ | [mm] | strain |
| $\varepsilon_o$ | [mm] | initial strain |
| $\varepsilon_f$ | [%] | flexural strain |
| $\varepsilon_{max}$ | [%] | maximum strain |
| $\sigma_f$ | [MPa] | flexural stress |
| $\sigma_{max}$ | [MPa] | ultimate stress strength |
| $\sigma_o$ | [MPa] | initial applied stress |
| $\tau$ | [s] | KWW relaxation time |
| $\emptyset$ | | KWW model |

This page was left intentionally blank

# Chapter 1 - Introduction

This chapter will explain the importance of studying the mechanical properties of adhesives used in adhesive bonded joints, the objectives necessary to define in order to successfully reach the goals stipulated and an overview of the dissertation structure.

## 1.1 Motivation

With the development and increase in usage of composites, it is possible to reduce significantly the weight of aircraft structures. However, the aeronautical industry is still being limited since it's still using the classic bonding technique also known as riveting.
An alternate bonding technique that has gained attention and traction recently is the adhesive bonding technique since it prevents local defects created by riveting and as a byproduct weight reduction. Due to certification conditions it is not viable to use adhesive bonded joints isolated which prevents us from taking full advantage of that technology [1].
In adhesive bonded joints the stress distribution is much more even than in the riveting counterpart which allows the structure to have a higher joint strength ultimately enabling the structure to bear a higher load before failing [2].
However, it was found that environmental conditions, mainly temperature and moisture, play a relevant role on the impact of mechanical properties [3]. Not only that but polymer-based materials are strain rate and load sensitive so the mechanical properties will also be affected by those conditions [4,5]. This means that adhesive bonded joints may fail when subjected to a load that is inferior to the ultimate load of the bonded joint.
So not only are the mechanical properties, such as flexural strength, flexural strain, ultimate stress strength and elastic modulus, important to understand the behavior of bonded joints, but also the viscoelastic properties, such as creep and stress relaxation, in order to have a better understanding of long-term stability and strength [6].
A better understanding of the adhesive bonded joints and more specifically the impact of the adhesive on the mechanical properties of the adhesive bonded joints is needed in order to allow a more generalized use of these type of joints in aeronautical structures and particularly in primary structures without constraints (e.g. certification conditions).
Due to what was mentioned before, this work will focus on characterizing the mechanical properties of the adhesive in order to have a better understanding of the impact of said factors in the mechanical properties.

## 1.2 Objectives

Characterize the viscoelastic and static mechanical behavior of a brittle adhesive, called SEAL® EA451.
Characterize the mechanical behavior of T-joints and how environmental degradation affects their performance.
In order to accomplish this, the following objectives must be achieved:

- Understand the functions, constraints and requirements of polymer composites used in aircraft structures.
- Characterize the viscoelastic behavior of the adhesive, namely:
- Static behavior in 3-point flexion.
- Strain rate.
- Creep behavior.
- Stress relaxation behavior.
- Understand the mechanical performance and failure modes of bonded joints in pull-off tests and environmental degradation impact on their performance.
- Write a report describing the state-of-the-art, motivation, experimental procedures and results analysis.
- Write a scientific report with a synthesis of the description of the state-of-the-art, experimental procedure and results discussion.

## 1.3 Dissertation Outline

This dissertation is organized in 5 chapters.
In the first chapter there is a short introduction why this topic is of interest, the objectives outlined for this dissertation and finally a brief description with the organization and description of the chapters.
In Chapter 2 the state-of-the-art is presented. In this chapter the theoretical knowledge needed to understand what is being studied is presented.
In Chapter 3 the type of materials used, the geometry of the specimens and their fabrication is described. It is also described the methodology used to obtain the results that will be analyzed in Chapter 4.

In Chapter 4 the presentation, analysis and discussion of the results obtained is done. This was done by comparing first the results between different test conditions, then by comparing control specimens with specimens that suffered environmental degradation and finally by comparing with known results and with the expected behavior mentioned in literature.

Finally, in Chapter 5 the conclusions are presented. This is divided in two parts one is the principal remarks made throughout the work such as advantages and disadvantages of fabrication methods and properties of materials and another part where suggestions are made on what could be done for future research.

This page was left intentionally blank

# Chapter 2 - State-of-the-Art

In this chapter the theoretical knowledge needed to understand and analyze the results that will be obtained in Chapter 4 is presented. It is divided in two subsections Composites and Adhesives.

## 2.1 Composites

### 2.1.1 Definition

A composite is a material that consists of a combination of two or more different materials, not miscible, with different properties in order to create a material with properties that are superior to the ones of its constituents [7,8].
The main components are the matrix and the fibers. Composites are usually classified in three different types: Laminate composites, sandwich composites and particle reinforced composites [7,8].
By selecting properties such as the constituent materials, the proportions and the geometrical arrangement it is possible to enhance the desired structural properties such as stiffness, strength or resistance in order to tailor the composite to meet specific design requirements. According to the design requirements composites different types of composites would be used. If it was pretended for them to have isotropic behavior then particle reinforced composite would be advisable. If on the other hand anisotropic behavior was the intended then laminate or sandwich composites would be the best choice [8,9].
Ever since the first applications of composites in aeronautics in the late 1960s in non-safety critical components we have seen an increase in the usage of components, first in military aircrafts and later in passenger aircrafts.

### 2.1.2 Advantages

This increase in usage is due to composites having advantages over the traditional materials such as low weight, integrated manufacture which is suited to produce one-piece structures leading to a reduction in weight and mechanical fasteners used, increase in structural efficiency since it is possible to tailor the composite to its specific function which leads to a possibility of optimizing to the maximum the design, high fatigue resistance allowing to reduce the maintenance costs and extending the operating life, corrosion resistance since unlike their aluminum counterparts composites such as carbon-fibers are immune to corrosion. Besides that it also has high radar absorption properties which makes them useful to use in stealth military aircraft, low thermal conductivity making them suitable for fighter aircrafts since they are more difficult to detect using radar and low coefficient of thermal expansion making them suitable for structures where it's needed stability since there is little to no expansion or contraction. However, the biggest advantage of composites is their specific strength which is much higher than that of a metallic counterpart [10,11].

### 2.1.3 Trend in Aeronautical Industry

Due to the reasons previously mentioned it is possible to not only observe an increase in usage of composites but also an increase in the usage of composites for primary structures. Nowadays composites can constitute as much as 40% of military aircraft and up to 50% of passenger aircrafts [10]. This trend is illustrated in Figure 1 where it is possible to observe an increase in the usage of composites throughout history.

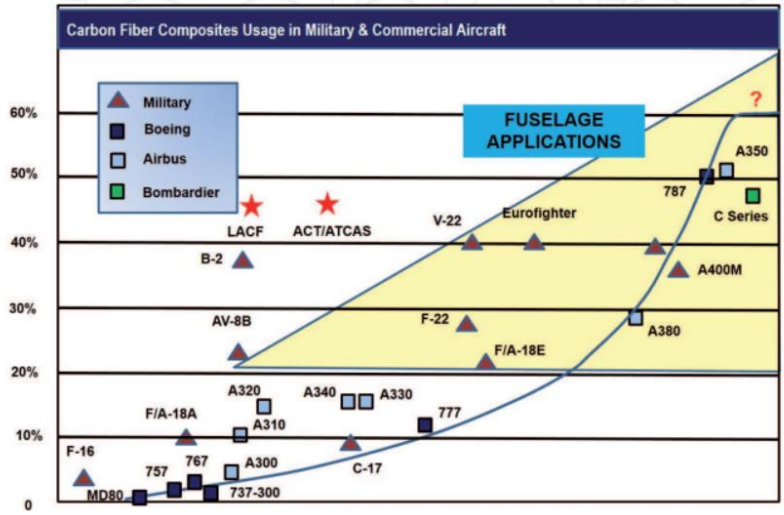

Figure 1 - Usage and Trend of CFRP in Military and Commercial Aircrafts [10].

This is the case for example of the Boeing 787 where 50% of the primary structure is made of composites [12] as shown in Figure 2 whereas for the Airbus A350 XWB the percentage of composites used is of 53% [13] as illustrated in Figure 3.

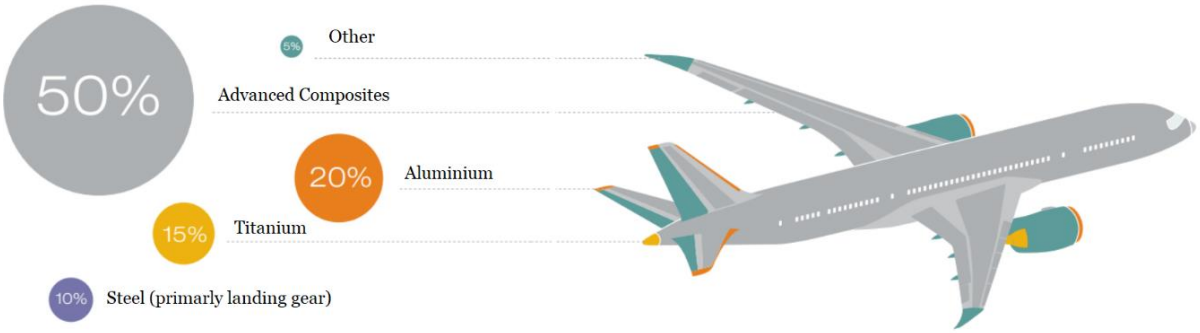


Figure 2 - Percentage of composites used in Boeing 787 and its location. Adapted from [12].

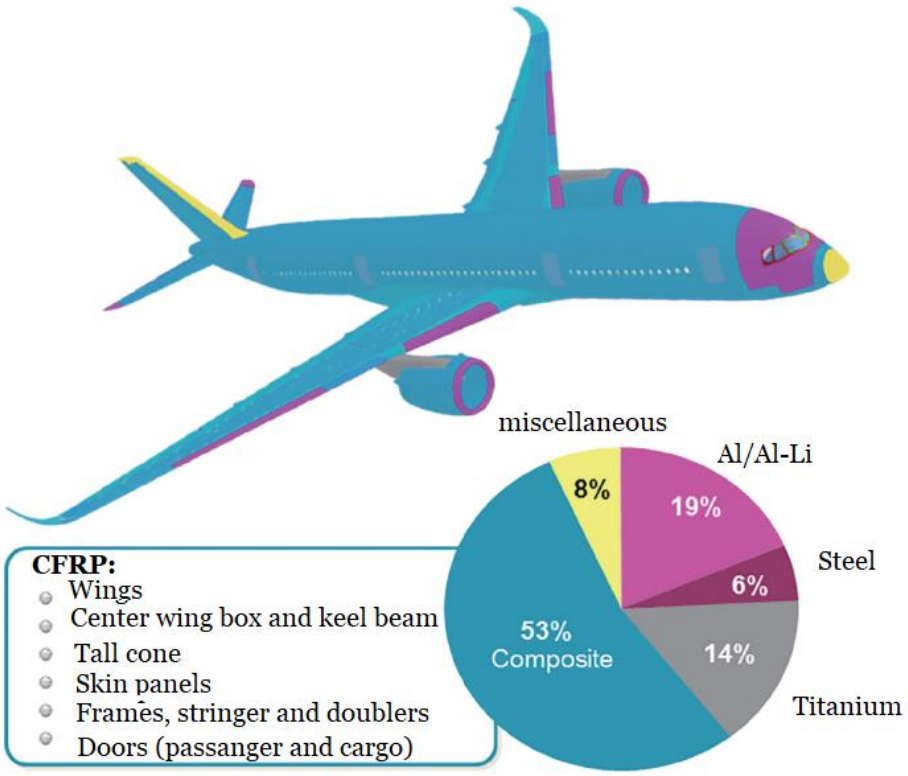


Figure 3 – Usage and localization of CFRP in Airbus A350 XWB. Adapted from [13].

### 2.1.4 T-Joints

T-joints are considered one of the typical joints that link two or more structural elements in order to transmit the load of perpendicular surfaces. They can also perform load transmission and bearing, achieving continuity of force transference and integrity of structural load distribution [14].
T-joints are used extensively in airplanes, automotive and in other areas to stiffen and connect structural elements [15].
The main advantage is the increase in bending stiffness of the structure with a minimal increase in weight. For this reason they are considered safety-critical components [16].

### 2.1.5 Disadvantages of Traditional Joining Methods

The types of joining methods commonly used for metals are welding and bolted joints [17], being one of the most common materials aluminum. However, both joining types come with disadvantages.
Welding methods lead to high residual stress, significant distortion and metallurgical defect and, for dissimilar metals, the formation of intermetallic compounds (IMCs) which results in poor mechanical strength [18,19]. For composite laminates, during the welding process, internal defects can increase due to the thermal decomposition of resin under long-term high-temperature condition which results in a reduction of bonding strength and as a consequence shear strength of the joint decreases ultimately leading to delamination [20].
Bolted joints generate local stress concentrations by drilling which introduces weak points due to high stress concentrations that could lead to crack initiation. Another thing to consider in drilling is that the fibers cut around the hole can no longer transfer the load. This means that strength degradation of the structure is unavoidable. Not only that but also weight gain by adding fasteners has to be considered in weight-sensitive structures such as aircrafts [20]–[22]. Finally, for metal-to-composite joints, galvanic corrosion is more likely. This effect is even more pronounced for small metallic parts, such as fasteners, in contact with large areas of CFRP resulting in an extremely high rate of galvanic corrosion [23].

### 2.1.6 Advantages of Adhesive Bonding

Adhesive bonding negates these disadvantages by ensuring a smooth stress distribution throughout the bondline increasing the overall strength of the joint as a consequence [2]. In Figure 4, it is possible to see how the presence or lack of weak points in a structure influences the stress distribution of a joint.
CFRP T-joints are increasingly being used in primary structures such as wing panels and fuselage sections, hence why they will be subject of focus in this dissertation [21,22].

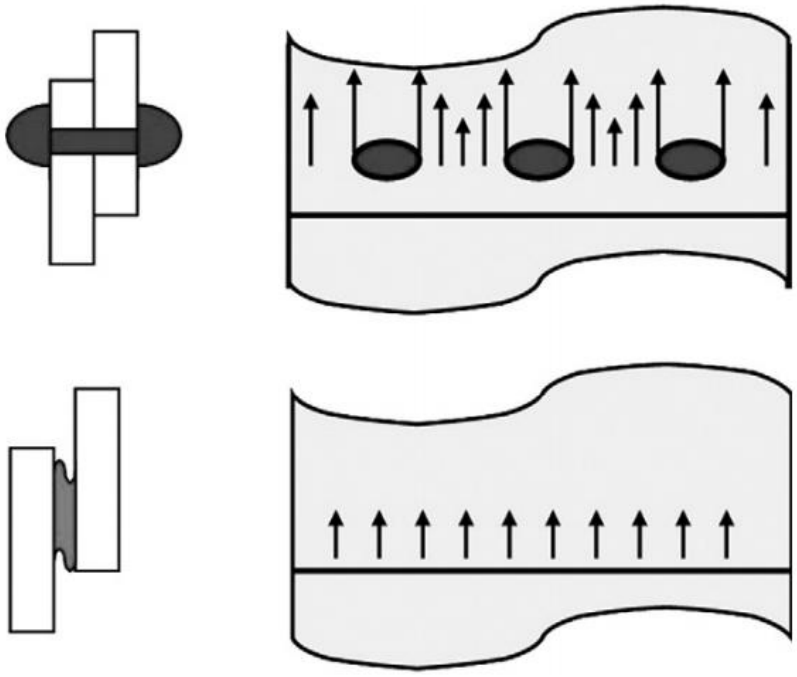

Figure 4 – Illustration of stress concentrations in riveted and bonded joints [66].

## 2.2 Adhesives

### 2.2.1 Applications

Adhesive bonding of primary structures in aircraft has been used for over 60 years and is still used nowadays as a direct alternative to riveting [26]. Its applications are extensive being used in diverse areas such as aerospace structures, electronics, mental and dental applications, civil engineering, between other [2], [27].

In the last 20 years, due to an increase in the use of composites, more attention has shifted towards this joining technology. This is justified by certain disadvantages of riveting when used in composites such as the breaking of fibers and the creation of local defects and residual stresses around the rivet hole. Since adhesive bonding nullifies these disadvantages it has been gained traction and has seen its usage increase in the last decades [26].

### 2.2.2 Adhesive Joint

An adhesive joint consists of: adherends, adhesive (or sealant), primer (if present, is optional), interphases and interfaces as can be seen in Figure 5 [28]. An adherend is a body that is, or is intended to be, bonded to another. An adhesive is the material applied to the surfaces of the adherends to join them permanently by an adhesive bonding process. Primers is a substance, or a mixture of substances applied before the adhesive to one or both of the adherends to be joined in order to improve adhesion and/or durability of the bond [29]. An interphase is a region between the adherend and the adhesive which has different properties from the bulk adhesive and the adherend [2]. Finally, the interface or boundary layer is the zone within the interphase that is in contact with the adjacent materials [28].

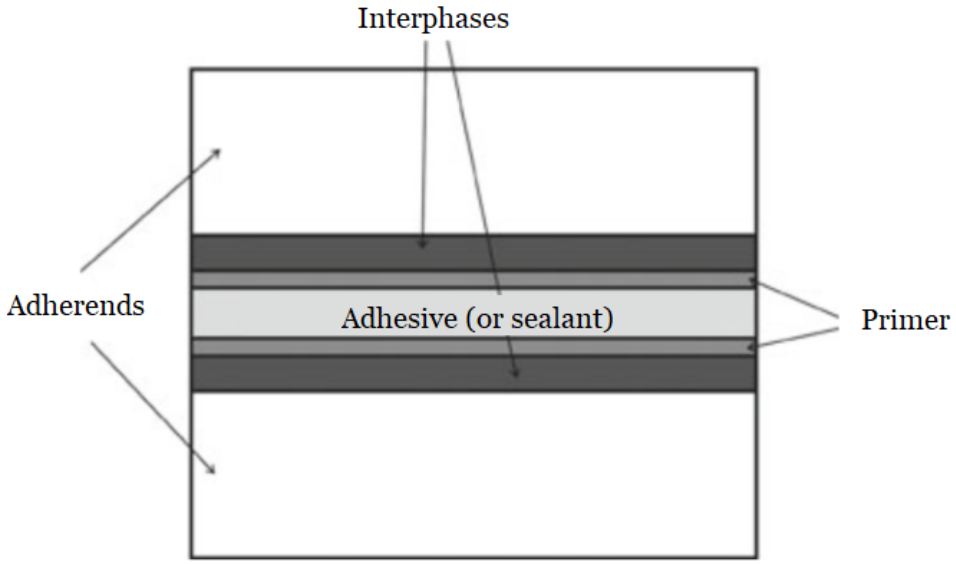


Figure 5 – Illustration of an adhesive joint system. Adapted from [25].

The factors that influence the bond strength are the surface preparation, joint configuration, adhesive properties and environmental conditions. The main factors to consider in environmental conditions are the temperature and moisture [30]. Exposure to elevated temperatures even for a short period of time might lead to irreversible chemical and physical changes in the adhesive. This is the most important factor to consider when designing a bonded joint since it has the biggest impact on the mechanical properties [3]. An increase in moisture has as consequences a reduction in the adhesive strength and stiffness and an increase in ductility. The combined effect of moisture and temperature (hydrothermal) conditions has been observed to be more damaging than the effects isolated however there is still a gap in knowledge about the impact on durability for bonded joints [30].

### 2.2.3 Types of Adhesives

It's possible to distinguish adhesives with brittle properties from adhesives with ductile properties. Brittle adhesives are characterized by presenting no plastic deformation and a linear response. Ductile adhesives are characterized by having a linear or almost linear response until the yield point stress also known as elastoplastic tensile instability point. After this point the adhesive suffers plastic deformation and consequently when the specimen is unloaded the material doesn't return to its original shape. In this plastic region it is necessary less stress to increase deformation [4].

Figure 6 shows the typical behaviors of a brittle and of a ductile adhesive in a stress-strain diagram where it is possible to observe the characteristics of the adhesives mentioned above.

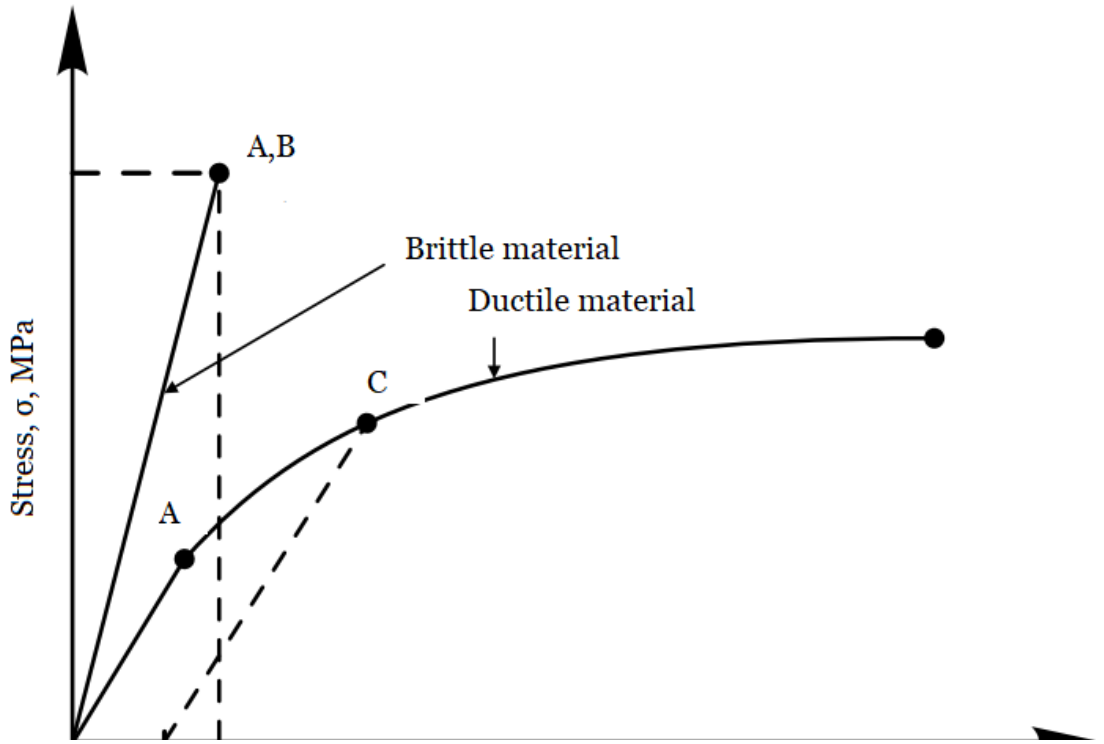


*Figure 6 - Typical stress-strain diagram for brittle and ductile polymers. A- Proportional limit, B- Rupture, C- Yield point. Adapted from [4].*

### 2.2.4 Characteristic Mechanical Response

For polymer-based materials stress-strain results can be affected by several factors, specifically strain rate and loading mode (unlike other materials such as metals).
This has to do with the fact that the response of these type of materials is viscoelastic and time dependent. The latter is an inherent property of these type of materials due to their unique molecular strength. With this in mind, it is important to not only determine the mechanical behavior of the adhesive, but also the viscous behavior since it is an important characteristic to predict the failure and lifetime of a bonded structure.
The studies usually done to determine how properties vary with time are creep behavior and stress relaxation tests [4,5].

Some studies have been done to try to comprehend the influence of the factors mentioned above and characterize the behavior in a joint. Two studies worth mentioning are Avendãno *et al.* [31], who studied the effect of temperature and strain rate on the maximum failure load, and Ilioni *et al.* [5], who proposed a viscoelastic-viscoplastic constitutive law to describe the mechanical behavior of a joint.

### 2.2.5 Characteristics of Brittle and Ductile Adhesives

Typically, brittle adhesives have a higher Elastic Modulus when compared with the ductile adhesives which makes them more suitable to be used as structural adhesives due to a higher joint strength, hence the reason why they have been preferred and why fewer investigations have been made on ductile adhesives [32]. However, certain characteristics make ductile adhesives more suitable in certain applications. When using stiff adhesives in dissimilar materials, premature failure may occur due to the different thermal expansion coefficients of the materials. One solution to prevent this is to use a ductile adhesive, however, with a decrease in joint rigidity [33]. Other important characteristics of ductile adhesives is their ability to resist dynamic loads when compared to stiff adhesives, as well as generating a more uniform stress distribution [31],[34].

### 2.2.6 Failure Modes

There are two basic distinct approaches to examine adhesive bonds: failure mode and fracture behavior. These approaches are complementary where the first ensures that the design is able to withstand the loads that the component is subjected to (without characterizing the fracture) and the second ensures that if debond occurs, it will not propagate to a point where catastrophic failure can occur by studying the propagation of the fracture.

Regarding the failure mode one criterion is that failure will occur when the maximum stress (or strain) within a bonded joint reaches a critical value. Bond failure often involves more than one failure mode and is described as a percentage of cohesive or adhesive failure, which is why slightly more sophisticated approaches acknowledge that failure criterion is met when some combination of stresses reach a critical value [27], [35].

According to the standard ASTM D5573-99 [36], when testing the bond in the tensile mode, in which two adherends are pulled apart in a direction perpendicular to the bond, an adhesively bonded joint can be subjected to six different failure modes illustrated in the Figure 7.

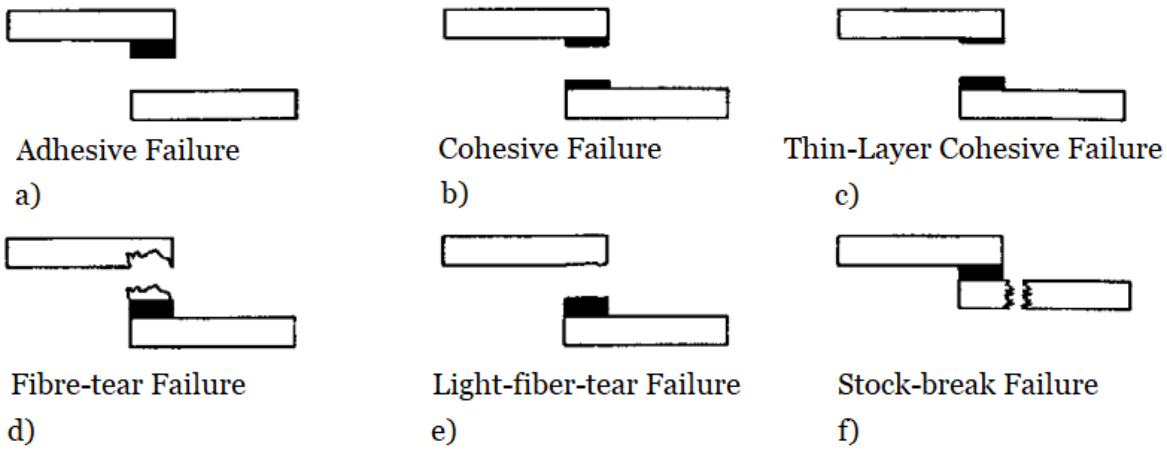


Figure 7 – Types of failure modes. Adapted from [37].

Thus, in summary, we have:

a) Adhesive failure or interfacial failure is when the rupture occurs in the interface adhesive-adhered.
b) Cohesive failure occurs when the separation is within the adhesive.
c) Thin-layer cohesive failure, also known as interphase failure is similar to cohesive failure, however, the failure is very close to the adhesive-adherend interface.
d) Fiber-tear failure occurs within the FRP matrix and is characterized by the appearance of reinforcing fibers on both ruptured sides on the surface.
e) Light-fiber-tear failure occurs on the FRP adherend near the interface and is characterized by a thin layer of the FRP matrix visible on the adhesive.
f) Stock-break failure is a rupture of the FRP adherend outside the adhesively bonded-joint region but often near it.

Fracture behavior enables us to interpret how the CFRP mechanical properties vary as the crack propagates [37].

There are 3 characteristic crack modes as shown in Figure 8 [38]:

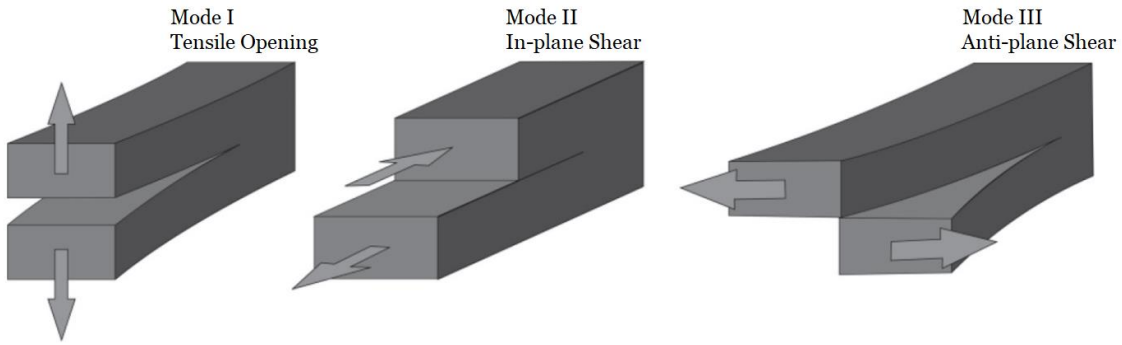


Figure 8 - Crack modes. Adapted from [38].

Thus, in summary:

- Mode I or tensile opening is characterized by an applied load that tends to create a peel displacement.
- Mode II is characterized by an in-plane shear stress.
- Mode III or anti-plane shear stress causes a shear displacement perpendicular to the displacement in mode II [39].
- Mixed-mode loading is the combination of at least two of these modes [40].

Due to physical and chemical interactions between adherends and adhesive as well as strain constraints due to the mechanical properties of the adherends, testing the bulk adhesive is not enough to provide adequate information about the behavior of the adhesive joint. It is also necessary to evaluate the behavior of the entire adhesive joint, not only individual testing of adhesives isolated from the system [41].

Applying these definitions of modes to a T-joint in an aeronautical structure it can be easily identified two crack modes in a typical failure sequence: I and II, as shown in Figure 9.

In this failure sequence shown in the figure, mode I can be observed in the initiation of the crack at the flange's tip. When the skin starts bending, mode II appears. Even though in comparison with mode I the load subjected in mode II is very small, the effects on the structure are quite noticeable making the fracture extend along the stiffener's foot [42].

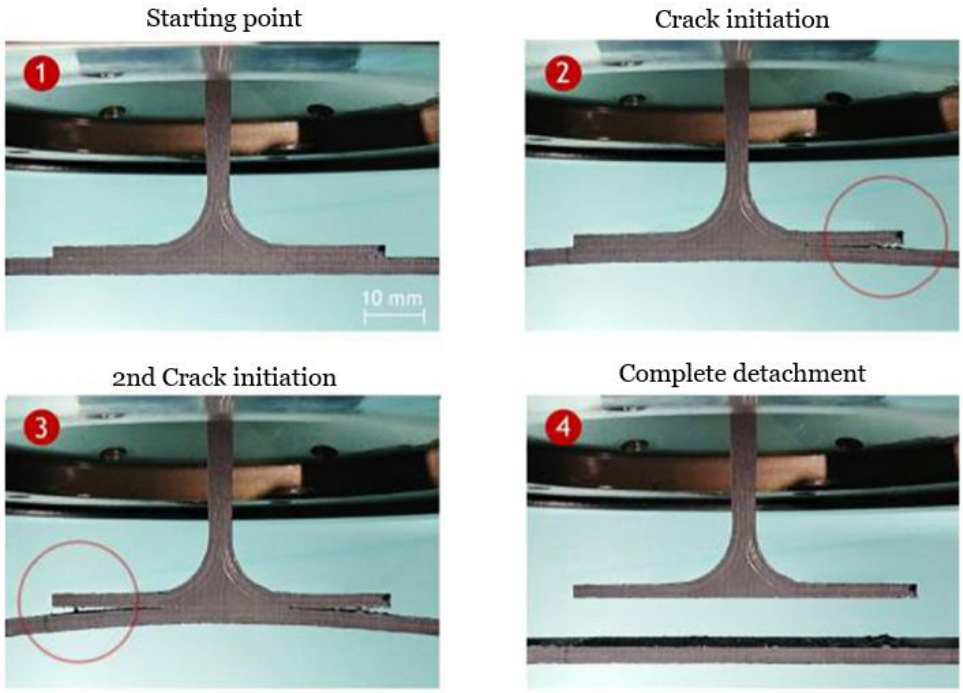


Figure 9 - Typical failure sequence in T-joints [39].

As mentioned before T-joints have been gaining traction in interest and use as shown in Figure 10 [43] where it can be seen the number of articles published each year. The information was taken from Google Scholar using the keyword “T-joints” and including patents and citations.

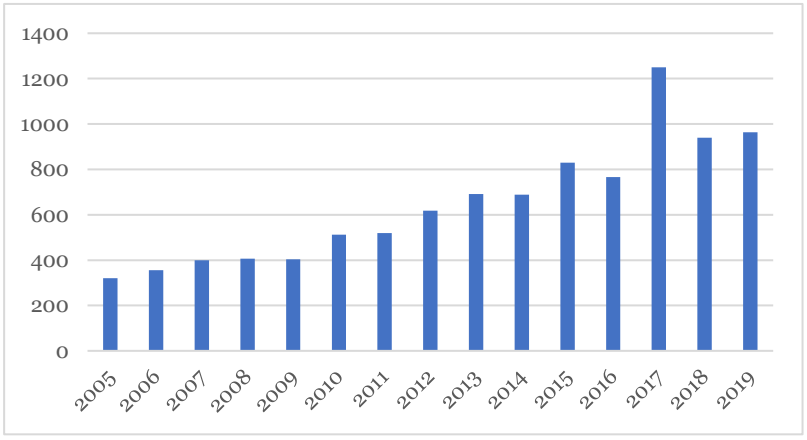


Figure 10 - Number of articles published about T-joints [40].

Some studies worth mentioning related to T-joints are described below.
Apalak and Davies [44] analyzed stress and stiffness of corner joints and found that tapering decreases peak stresses at critical points. In addition, they also found that an increase in adhesive thickness leads to a significant decrease in stiffness.

Khalili *et al.* [45] studied using numerical analysis and confirming with experimental data the effect of filler geometry and core material of sandwich on the performance of the T-joint and found that the best angle of core triangle is of 45 degrees and the core material of the sandwich panel has a direct relation with the joint failure load.

Burns *et al.* [15] studied novel designs approaches of CFRP T-joints and was able to increase up to 125% the damage initiation load under bending load and up to 85% the tensile loading when compared with the quasi-isotropic design.

Hou *et al.* [46] investigated the influence of joint geometry and transverse speed on tensile properties of T-joints by fabricating 3 different geometries and subjecting them to T-pull tests concluding that the T-joint had the best results out of all different geometries.

Dharmawan *et al.* [47] investigated the effect of the geometry of a T-joint on the strain distribution and found that: the skin thickness and stiffener's angle affected the critical strains; the presence of disbond altered distribution of axial strain through the thickness of the stiffener and that the disbond caused otherwise relatively uniform axial strain to vary linearly through the thickness of the stiffener.

Burns *et al.* [48] researched how to strengthen composite T-joints under bending load using bio-inspired design which led to a higher bending failure initiation load (of about 40%) and a higher elastic strain energy capacity (around 75%) when compared to a base T-joint without increase in weight or costs.

Ma *et al.* [14] studied the interface debond initiation and evolution for CFRP T-joints under quasi-static load using active Lamb-wave-based damage with piezoelectric sensor and was able to detect invisible debond damage initiation as well as record the whole process of failure propagation.

Shenoi and Violette [49] examined the influence of geometry on the ability to transfer out-of-plane loads in a T-joint and were successful in developing a design tool to predict failure mode.

Theotokogou *et al.* [50] examined non-linear deflection response of highlight stressed sandwich T-joints and found that, the behavior is characterized by geometric non-linearities due to high out-of-plane loads and by material non-linearities due to materials that yield in a plastic fashion and, that there two different failure initiation mechanism in a T-joint where it can either start in the tip of the flange or in the core.

Li *et al.* [51] analyzed stresses of T-joints under different loading conditions and found that when the joint is subjected to a load in the direction illustrated in the Figure 11, maximum normal stresses concentrated on the edge of adhesive layer joint appear and this is where the first failure appeared.

Figure 11 - Load mode typically applied in T-joint.

Kesavan *et al.* [52] developed a Structural Health Monitoring (SHM) system for 2d polymetric composite T-joints and was successful in not only detecting the presence of damage but also the size and location in complex composite structures examining strain distribution of structure under operational loading.
Whittingham *et al.* [53] also developed a SMH technique for T-joints however this was done by measuring the response of piezoelectric actuators to identify alterations in structural properties such as stiffness and damping.
Yap *et al.* [54] was able to develop a Finite Element (FE) Analytical tool for rapid and accurate damage assessment of debonds in composite stiffened parts (including T-joints).
Finally, Blake *et al.* [55] investigated the static structural response on a T-joint containing viscoelastic inserts and was successful in developing a progressive damage model by validating it with experimental data.
Concerning adhesives, there has been a focus on improving bondline strength by using a combination of two or more adhesives. This has been reported by several authors as an alternate technique to improve stress distribution and increase joint strength by reducing peel stresses at the edges of the joint [30,31], [53]–[57].
Finally, Akpinar *et al.* [41] studied the stress distribution in bi-adhesively bonded T-joints and found a reduction in peel stresses and an increase in joint strength (by 20%) when compared with adhesives used separately, making this a valid technique to increase T-joint strength.

Due to the geometry of the joint configuration, the laminated construction and the overall adhesive-adherend interaction of T-joints, hydrothermal exposure has a particular effect on this type of joints, as mentioned in studies done by Rao *et al.* and Kumari *et al.*
Rao *et al.* [61] states that for T-joints subjected to hygrothermal conditions the ultimate failure load is correlated with the thickness of the skin. This is due to thinner specimens being more susceptible to hygrothermal exposure.
Kumari *et al.* [62] found that for Graphite/epoxy T-joints the skin-stiffener interface is a critical zone for failure due to an increase in high transverse normal and shear stresses when subjected to hydrothermal conditions.

This page was left intentionally blank

# Chapter 3 – Experimental Procedure

This chapter is divided into two subsections. The experimental setup mentions the characteristics of the materials used and why they were chosen, the dimensions of the specimens and how they will be fabricated. The experimental methodology mentions the machines used, the test conditions and procedures used to obtain the results that will be mentioned in Chapter 4.

## 3.1 Experimental Setup

### 3.1.1 Materials

3.1.1.1 Adherends

The adherends chosen were made from HS160 REM, from manufacturer Composite Materials Italy, batch number 120014045. It is a UD (Unidirectional) tape, 60 cm wide, has a length of 100 m and is 0,164 mm thick. The Tg is of 125ºC and the manufacturer supplies a table with the mechanical properties of the material, shown in Table 1 [63].

Table 1 - Mechanical properties of HS160 REM [63].

| **Cured Material Property** | **Unit** | **Actual Values** |
|---|---|---|
| Tensile Modulus 0º | GPa | 123 |
| Tensile Strength 0º | MPa | 2294 |
| Tensile Strain | % | 1.72 |
| Compression Modulus 0º | GPa | 109.8 |
| Compression Strength 0º | MPa | 1152 |
| Flexural Modulus 0º | GPa | 134 |
| Flexural Strength 0º | MPa | 1850 |
| Inter-laminar Shear Strength | MPa | 81.5 |
| Cured Ply Thickness | mm | 0.164 |

### 3.1.1.2 Adhesives

The adhesive chosen was SEAL® EA451 U150 (unsupported), a structural epoxy adhesive film. This is a brittle adhesive manufactured by Composite Materials Italy®, batch number 120003727. It is 100 cm wide and 0.125 cm thick.

As mentioned in the datasheet it is of interest because it has a flexible cure temperature ranging from 90°C to 180°C allowing for different types of cures such as co-cure and secondary bonding of composite substrates which is ideal since the fabrication method of the T-joint relies on secondary bonding. It has a Tg of 190°C [64].

The tensile mechanical properties were obtained by João V. Cardoso *et al.* [42] and are represented in Table 2.

Table 2 - Tensile mechanical properties of adhesive [42].

| $\sigma_{max}$ [MPa] | $\varepsilon_{max}$ [%] | E [GPa] |
|---|---|---|
| 28.9±12% | 0.4±12% | 7.5±3% |

The viscosity profile is shown in Figure 12. This information is supplied by the manufacturer in the TDS [64]. Taking the viscosity profile into account the temperature of 120°C was chosen for the fabrication process due to it being where the viscosity is minimal.

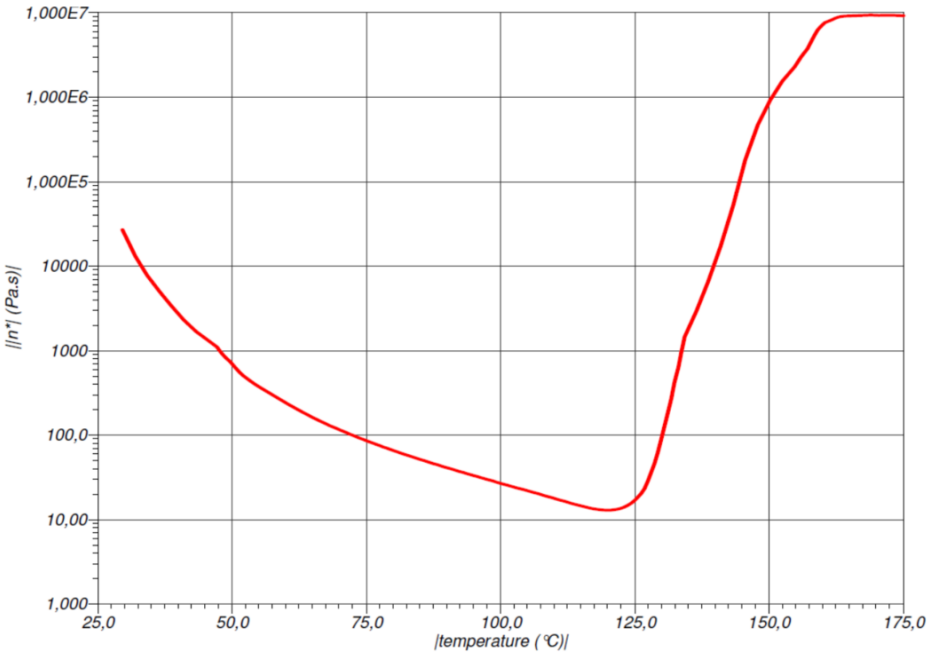


Figure 12 - Viscosity profile of adhesive [64].

### 3.1.2 Specimens

3.1.2.1 Bulk Adhesive Characterization

Since the T-joints were subjected to bending tests the adhesive was characterized using the ASTM Standard D790-03 [65] to obtain the flexural properties. Taking this into account the final dimension of the specimens was of 72 x 15 x 2 mm as shown in Figure 13.a). These dimensions were chosen to comply with the Standard mentioned above as well as aiming to minimize the material used in order to save/maximize the resources available.

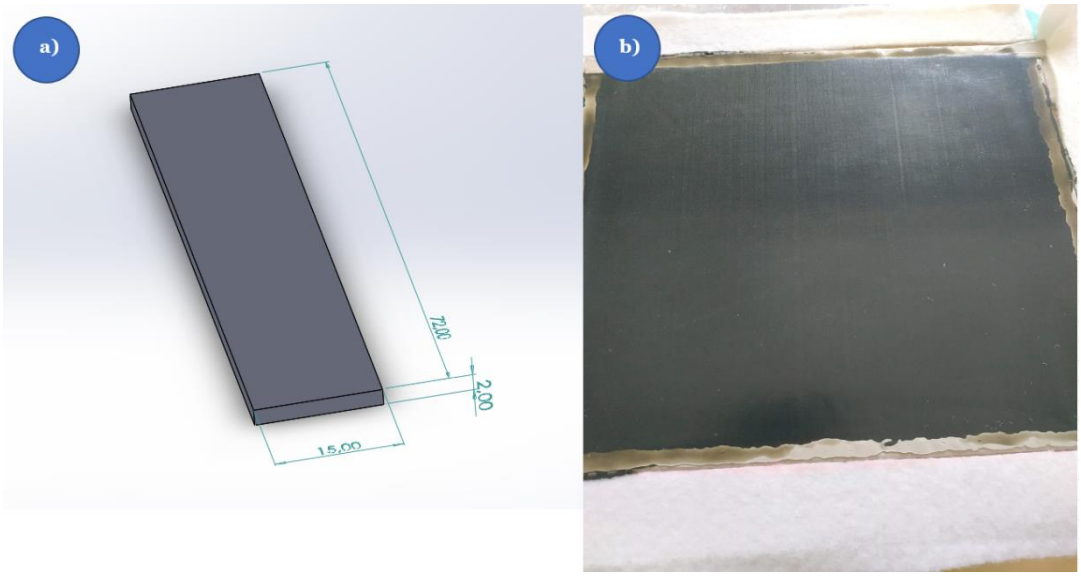


Figure 13 – Bulk adhesive: a) Specimen's dimensions; b) Laminate.

3.1.2.2 Skin-to-Stiffener Joint

The skin-to-stiffener joint is composed of two parts, the skin and the stiffener. The skin dimension was of 260 x 40 x 2.624 mm. The stiffener's dimensions are represented in Figure 14.

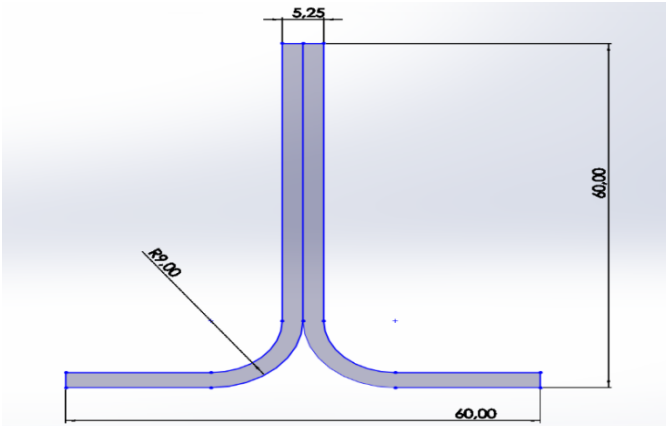


Figure 14 - Stiffener's dimensions.

### 3.1.3 Fabrication

3.1.3.1 Bulk Adhesive Characterization

In order to characterize the adhesive first the fabrication of the bulk adhesive had to be done. This was done by the following procedure:

1. A metal plate tool was covered with Teflon® sheet, using high temperature tape to hold the Teflon in place.
2. The adhesive roller was taken out of the freezer, waiting a short period of time before cutting it (the best time was found to be around 5 minutes). This is due to being the best compromise found between stiffness (when in the freezer) and tack (at room temperature).
3. Using a box cutter, the plies were cut in the desired dimension.
4. The first ply was placed in the metal plate tool. Manual pressure was applied during the lay-up of the adhesive plies to minimize the appearance of voids.
5. Every 3 plies the other metal plate tool was placed on top covered with Teflon® sheet and
   100 bars of pressure with the hydraulic press were applied.
6. After applying the last ply, vacuum tape was employed around the adhesive to prevent it from leaking. Then the laminate was covered with another Teflon® sheet and a layer of polyester breather (Airweave® N10) to provide airflow under vacuum and finally placed inside a bagging film (Stretchlon® 700) and sealed using a heat-sealing machine (Lovero SK-510).
7. The whole set was taken to the autoclave with a temperature of 120ºC. The cure cycle that yielded the best results was to begin with vacuum until the temperature of the autoclave reached 70ºC, then 2 bars of pressure were added and the vacuum valve closed. Finally, the rest of the procedure was made without any change in pressure or vacuum.
8. It was allowed to cool down for at least 6 hours without opening the autoclave in order to prevent thermal shock or introduce residual stress in the material. In Figure 13.b) the bulk adhesive is shown after being taken out of the autoclave.
9. The CNC water jet cutter (Pronum WaterJet 3015) was used to cut the plate into the dimensions specified, making sure they complied with the standard.

3.1.3.2 Skin-to-Stiffener Joint

The fabrication of the CFRP skin-to-stiffener joint was done by the following procedure, as described in the literature [66]:

1. A metal plate tool was covered with Teflon® sheet, using high temperature to hold the Teflon in place.
2. Using a box cutter, the plies were cut in the desired dimension.
3. Hand-layup of the plies was done by the following stacking sequence $[-45^{o},0^{o},45^{o},90^{o},90^{o},45^{o},0^{o},-45^{o}]_{s}$ in order to obtain a quasi-isotropic behavior. For the skin 16 plies were used, for the stiffener 32.
4. Slight heating of the plie and manual pressure were applied during the lay-up in order to minimize the appearance of voids and improve adhesion.
5. After applying the last ply, polyester breather (Airweave® N10) was employed to provide airflow under vacuum and absorb the excess resin. Then the laminate was placed inside a bagging film (Stretchlon® 700) and sealed using a heat-sealing machine (Lovero SK-510).
6. The set was taken to the autoclave with a temperature of 120°C, vacuum and an initial pressure of 1 bar. When the temperature got to 80°C the pressure was increased to 5 bars and no further changes were done throughout the cure cycle.
7. It was allowed to cool down for at least 6 hours without opening the autoclave in order to prevent thermal chock or introduce residual stress in the material.
8. The Struers Accutom-2 precision saw machine was used to cut both the skin and the stiffener into the dimensions specified.
9. Both the skin and the stiffener where polished using 120 grit paper in order to avoid stress concentrations due to surface irregularities and cleaned with alcohol before applying 5 plies of adhesive in order to ensure the best bonding quality possible.
10. Finally, the whole set was taken to the autoclave on a bagging film and with breather and subjected to the same cure cycle as the bulk adhesive. Once more when it finished it was allowed to cool down for at least 6 hours without opening the autoclave. In Figure 15 it is shown the specimen obtained.

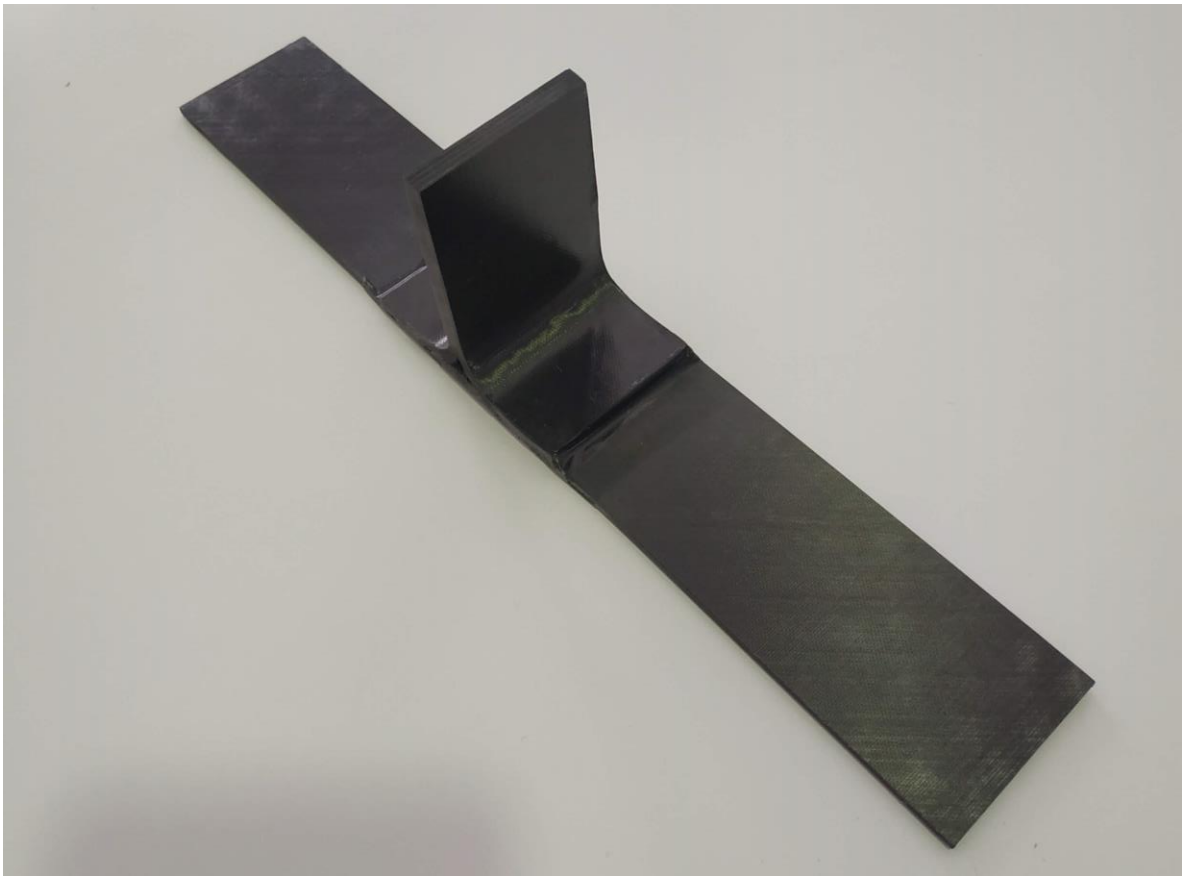

Figure 15 - T-joint specimen.

## 3.2 Experimental Methodology

### 3.2.1 Bulk Adhesive Characterization

The experiments to obtain the mechanical and viscoelastic properties of the bulk adhesive were conducted on a Shimadzu universal testing machine with a maximum load of 10kN where load, displacement and strain data were acquired.
The parameters of the experiment such as displacement rate and maximum stress were configured depending on the goal.
In order to obtain the mechanical properties of the adhesive, ASTM D790-03 Standard [65] was followed and a strain rate of 2mm/min was set.
Having the data acquired by the machine it was possible to calculate the mechanical properties of the adhesive by using the following equations found in the ASTM D790-03 Standard:

The first thing needed to know was the span which can be calculated with the following equation:

$$L = 16d \tag{1}$$

Where L is the support span and d is the depth, in mm, of the specimen. The flexural stress can be calculated using the following formula:

$$\sigma_f = 3\frac{P_l L}{2bd^2} \tag{2}$$

Where $\sigma_f$ is the flexural stress at midpoint in MPa, $P_l$ is the load at a given point in Newton and b is the width (mm) of the specimen. The flexural strain is calculated by the following formula:

$$\varepsilon_f = \frac{6Dd}{L^2} \tag{3}$$

Where $\varepsilon_f$ is the flexural strain normalized and D is the deflection on the center of the beam (mm). Finally, the Elastic Modulus is given by the following equation in MPa:

$$E_B = \frac{L^3 m}{4bd^3} \tag{4}$$

To obtain the behavior of the adhesive for different strain rates, 5 different strain rates were tested using a logarithmic sequence. They were the following: 0.02, 0.2, 2, 20, 200 [mm/min].

For creep and relaxation stress tests 3-hour experiments were done for each specimen. For stress relaxation the displacement applied was the corresponding to 60%, 50%, 40% and 20% of the ultimate stress strength, as in accordance with the Standard ASTM D2991 [67]. For creep tests four different percentages of load were applied for each type: 60%, 50%, 40% and 20% of the ultimate stress strength of the adhesive, as in compliance with the Standard ASTM D2990-17 [68]. The initial strain rate for both types of testes was of 2 mm/min.

The Creep Compliance function is used to determine whether the response of the material is linear or not. The function is given by the following equation in $GPa^{-1}$:

$$D_f(t) = \frac{\varepsilon(t)}{\sigma_0} \tag{5}$$

As a means to conclude that the response of the material is linear, the compliance function must be independent of stress level [4].

In order to predict the viscoelastic behavior of the bulk adhesive two methods were used: KWW for stress relaxation and Findley's law for creep behavior. According to the literature these are the models that have the best compromise between reliability and complexity.

The KWW (Kohlrausch-Williams-Watts) model is given by the following function:

$$\emptyset = \frac{\sigma(t)}{\sigma_0} = e^{-\left(\frac{t}{\tau}\right)^{\beta}} \quad (6)$$

Where τ is the KWW relaxation time and β the degree of non-exponentially of the function. The KWW model could also be applied to predict creep behavior however the Findley method as shown to provide better results for long-term prediction which is why this model was chosen instead [69]. Findley's law for creep behavior is given by:

$$\varepsilon(t) = \varepsilon_0 + At^n \quad (7)$$

Where A is the amplitude of transient creep (time-dependent) and n is a constant independent of stress.

Two types of specimens of bulk adhesive were fabricated to be tested: the control group and the ones that suffered environmental degradation.

In order to induce an environmental ageing in the specimens by subjecting it to hydrothermal conditions three different conditions were created. For the first condition the specimens were immersed in water at room temperature (~20ºC). For the second condition the specimens were immersed in water at 40ºC. Finally, for the third condition the specimens were immersed in water at 80ºC. Moreover, these environmental conditions are within the service parameters to which an aircraft may be exposed.

Periodical weight measures were done using an Oertling VA204 scale in order to evaluate the evolution of apparent porosity and the bulk density, in compliance with the Standard ASTM C 20 [70]. Before weighing specimens', the surface was cleaned with paper in order to remove water that was attached as a way to prevent errors induced by extra weight of the water particles.

In order to calculate the apparent porosity and the bulk density, first the exterior volume had to be calculated. This was done by using the following equation:

$$V = W - S \quad (8)$$

Where V is the exterior volume in $cm^3$, W is the saturated weight and S is the suspended weight, both in grams (g). Knowing this we can calculate the apparent porosity with the equation:

$$P_a = \left[\frac{W - D_w}{V}\right] . 100 \quad (9)$$

Where P is the apparent porosity in percentage and $D_w$ is the dry weight in grams. Finally, the bulk density (B, $g/cm^3$) of the adhesive can be obtained using the equation 10:

$$B = \frac{D_w}{V} \tag{10}$$

The specimens were kept immersed until the maximum apparent porosity was achieved for the specimens kept at 80°C. Finally, these specimens were also tested using the same methods described above.

### 3.2.2 Stiffener Pull-Off Test

The experiments to obtain the mechanical and viscoelastic properties of T-joints were conducted on an Instron 8800R1341 universal testing machine where load and displacement data were acquired. This was done at room temperature with a span of 185 mm and a strain rate of 2 mm/min. The tests were recorded. After failure the T-joints were examined to determine the reason that led to failure (failure mode) and pictures were taken of both the skin and stiffener.
Two types of specimens were tested, the control group and the ones that like the bulk adhesive suffered ageing by being kept at 80°C and immersed until they had reached the maximum apparent porosity.

# Chapter 4 – Results and Discussion

In this chapter will present the results obtained and analyze them for the Bulk Adhesive and for the Stiffener Pull-Off Tests (SPOT). This chapter links directly with Chapters 2 and 3 since both theoretical knowledge to interpret the results and practical knowledge to fabricate and test the specimens are needed in order to obtain and analyze the results.

## 4.1 Bulk Adhesive Characterization

According to literature some of the typical adhesives used in civil aircraft structures are: AF 191, AF 163-2, Redux 319 and Araldite AV 138 [71]. In order to judge whether the adhesive is a good choice to be used in aircraft structures the mechanical properties were extracted from TDS (technical datasheets), articles and dissertations and compiled in Table 3 shown below [42], [72]–[75].

Table 3 - Tensile mechanical properties of adhesives commonly used in aircraft structures [42],[ 72-75].

| **Adhesive** | **$\sigma_{max}$ [MPa]** | **$\varepsilon_{max}$ [%]** | **E [GPa]** |
|---|---|---|---|
| EA451 | 28.90 | 0.40 | 7.50 |
| Araldite AV 138 | 41.01 | 1.30 | 4.59 |
| AF 191 | 13.00 | 2.11 | 0.71 |
| AF 163-2 | 48.26 | - | 1.10 |
| Redux 319 | 43.20 | - | 2.19 |

From the table it is observed that the adhesive when compared with others has a very high elastic modulus, has considerable tensile ultimate stress strength and very little maximum strain. This makes it like a good choice to apply in aeronautical structures however, it is worth mentioning that the fact that it has very brittle behavior makes it more likely to have high stress concentrations on the edges which could lead to premature failure. The way to take full advantage of the properties of this adhesive would be to mix it with a ductile adhesive in order to prevent those high stress and increase the overall joint strength [33].

In regards to obtaining the flexural mechanical properties, the fabrication of the bulk adhesive was an iterative and interactive process where, several fabrication methods were tried in order to obtain the best mechanical properties with the lowest standard deviation possible. What showed to have the greatest influence in the mechanical properties of the bulk adhesive was the appearance of voids leading to premature failure. The fabrication characterized in Chapter 3 is the one found to lead to the minimization of voids.
All the following results presented were obtained using that fabrication method.
For the static bending tests, the stress-flexural strain curves were obtained. The typical behavior of this adhesive for the displacement rate mentioned in Section 3.2 (2 mm/min) is shown in Figure 16. A fracture surface analysis was conducted for each specimen in order to determine the point where the crack initiated, the mode and possible causes (such as voids) as a way to discard faulty specimens. Typical faulty specimens showed a crack initiation in a void instead of in the outer edge where maximum stress is expected.

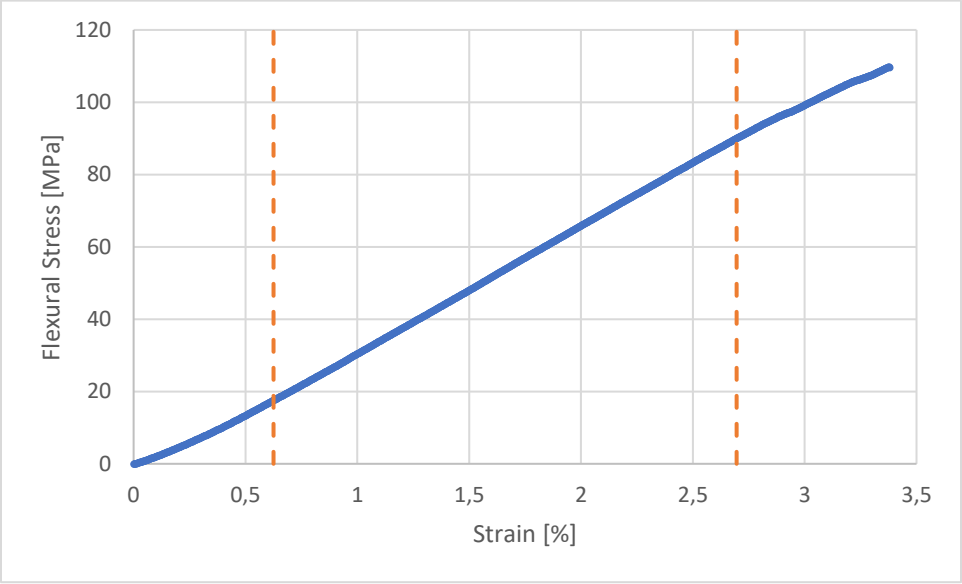


Figure 16 – Characteristic flexural stress-strain curve of adhesive.

This curve has 3 distinct regions: The toe region (initial), the linear region (middle) and the pretransition region (final). The separation of the regions is represented by the vertical lines. The toe region appears due to slack and position of the specimen meaning no results can be extracted from this part. The linear region is from where, in compliance with the ASTM D790-03 Standard, mechanical properties can be calculated [65]. Finally, the last region also known as pretransition region is a region where there is a change in topological structure which will influence the elastic properties [76].

From the figure it can be observed that the adhesive has a brittle behavior. The flexural mechanical properties obtained are shown in Table 4.

Table 4 - Flexural mechanical properties of the adhesive.

| $\sigma_{max}$ [MPa] | $\varepsilon_{max}$ [%] | E [GPa] |
|---|---|---|
| 104±9.5 | 3.17±9.4 | 2.38±6.6 |

The properties shown in Table 4 were obtained by testing a minimum of 6 specimens that were considered to be valid results (some specimens with defects in fracture surface were discarded). With this number of specimens, it was possible to obtain the mechanical flexural properties of the adhesive with a reduced standard deviation, presented in the table in percentage. The ultimate stress strength of the adhesive was found to be of 104 MPa, the maximum strain of 3.17% and the Elastic Modulus of 2.38 GPa. Worth mentioning that in literature the adhesives properties are usually obtained through tensile testing so no information about adhesives with the same or similar use is available to compare.

For the different strain rates, the properties obtained are represented in Figure 17.

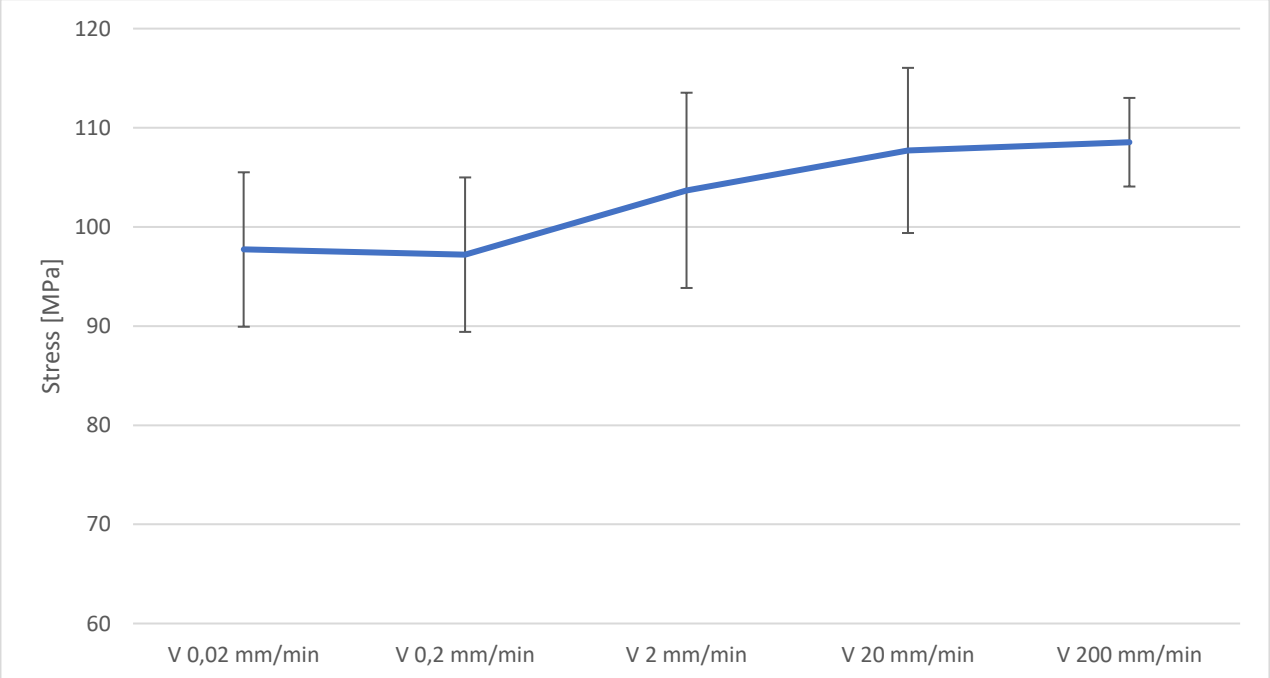


a) Ultimate stress strength

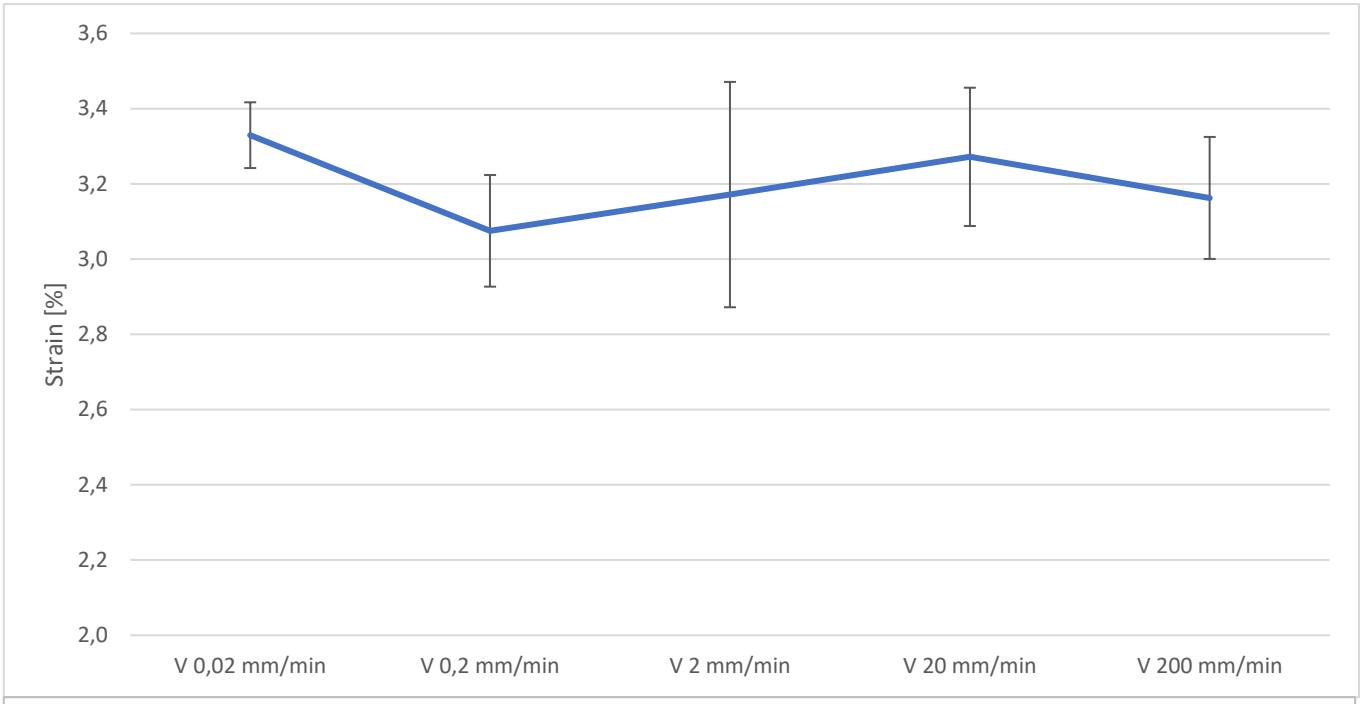


b) Maximum strain

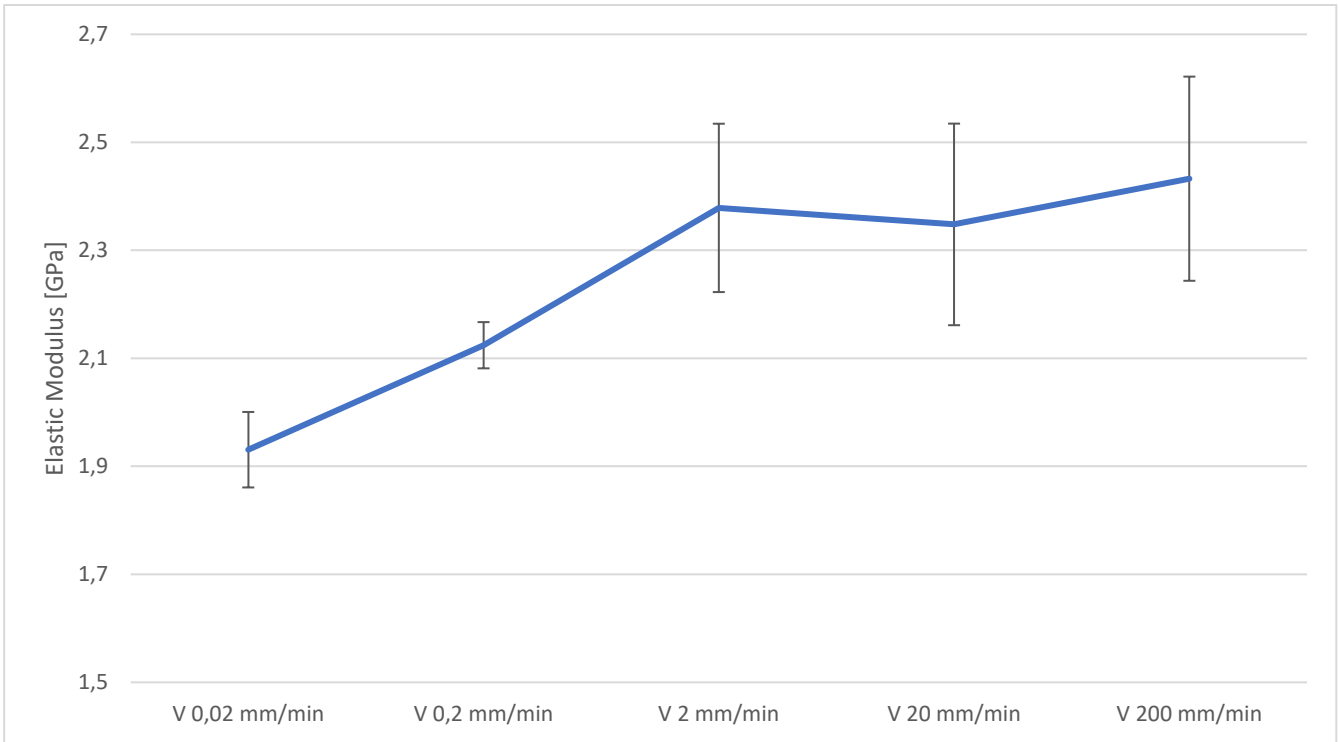


c) Elastic Modulus

Figure 17 - Variation of flexural mechanical properties with different strain rates.

From the results obtained it is possible to notice that, with an increase of the strain rate, an increasing trend in the ultimate stress strength. This is the expected trend for polymers and has been described in literature by Reis *et al.* [77] due to an increase in stiffness since there is less time for chain or rotation movement. For the maximum strain the trend is not well defined and therefore no tendency is noticeable as it appears to be independent of the strain rate. Usually, the reported trend is that the maximum strain decreases as the strain rate increases. This decrease is justified by the increasing stiffness which makes the polymer more rigid thus achieving less maximum strain. The Elastic Modulus increases as the strain rate increases. This is supported by literature where it is shown that the tendency for polymers is to increase as strain rate increases [78]. As mentioned for the ultimate stress strength this increase in the Elastic Modulus is a consequence of the increase in stiffness of the polymer. These results show us that the adhesive is strain-rate sensitive.

For creep and relaxation tests the stress percentages chosen were done by analyzing the flexural stress-strain graph and observing that the transition from the elastic region to the pretransition region happens around 80%. Since the creep and relaxation tests have to be done in the elastic region the values chosen had to be lower than that.

In order to evaluate if the material is linear viscoelastic one of the following two conditions must be met. The condition necessary to check for the relaxation test is whether the Relaxation Modulus is the same for the different stress levels at any given time.

For the creep test the condition necessary to verify is whether the Compliance is independent of the stress level at any given time [4]. If the conditions are true then predictive models can be applied.

In Figure 18 it is possible to observe the Compliance curves for the 3 lines obtained for each stress percentage.

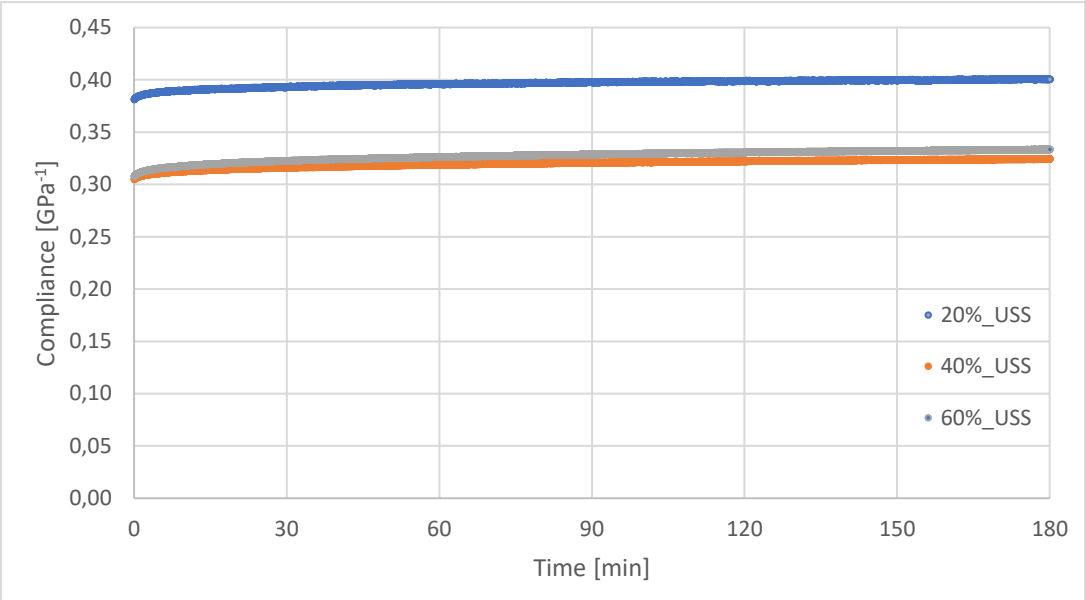


Figure 18 - Compliance creep curves for different percentages of USS.

From the Figure 18 we can assume that the material has linear viscoelasticity characteristics since the values are very close to each other, leading us to believe that the small differences are most likely due to external noise or small experimental differences, such as different room temperature rather than a non-linear property of the adhesive. This means that by knowing the creep compliance function it is possible to characterize the viscoelastic response of the adhesive by applying models such as KWW and Findley [74,75].

In Figure 19 the average normalized stress relaxation curves (obtained by dividing the stress at each moment by the initial one) are represented for a test time of 180 minutes.

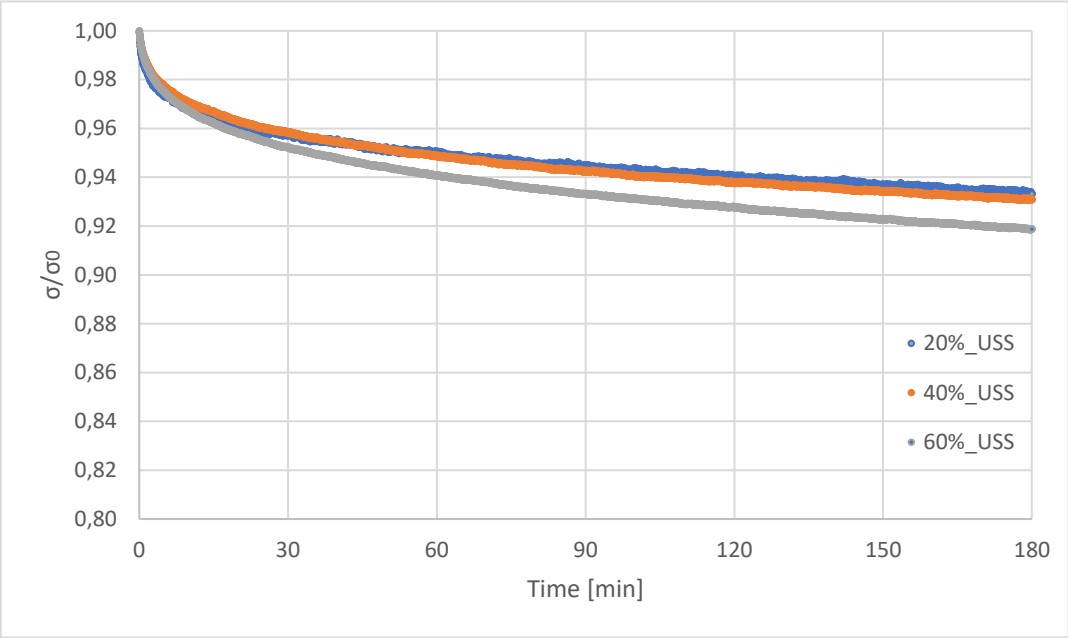


*Figure 19 - Average normalized stress relaxation curves for different percentages of USS.*

The average curve that corresponds to 20% of the ultimate stress strength (USS) has more oscillations due to external noise. A rapid initial decrease in the tension is seen for all the curves, being more accentuated for the curve 60%_USS. While for the 20%_USS and 40%_USS the results are quite similar, for the 60%_USS curve the difference is more noticeable. All curves seem to have a tendency to stabilize to a certain stress however the test length is not long enough to fully see this effect.

This rapid initial decrease behavior is common and has been mentioned in literature. Some studies worth mentioning that refer to this tendency were done by Reis *et al.* [81] and Ferreira *et al.* [82]. The fact that the stress decrease is more accentuated for the specimens subjected to a higher stress is also mentioned by Reis et al. [77].

For the initial region where the stress decrease is higher, for the curve corresponding to 60% of the ultimate stress that decrease is of almost 5% while for the rest of the test is only of around 3%. On the other hand, for the curve corresponding to 20% of the ultimate stress that decrease is of around 4% while for the rest of the test is only of around 2,6%. This proves that the stress decrease is dependent on the initial stress level.

In Figure 20 two curves are represented for stress relaxation tests. The curve obtained by the average experimental data for 50% of the USS, as well as the maximum and minimum values obtained for the final instant, and the theoretical data obtained by fitting the KWW model.

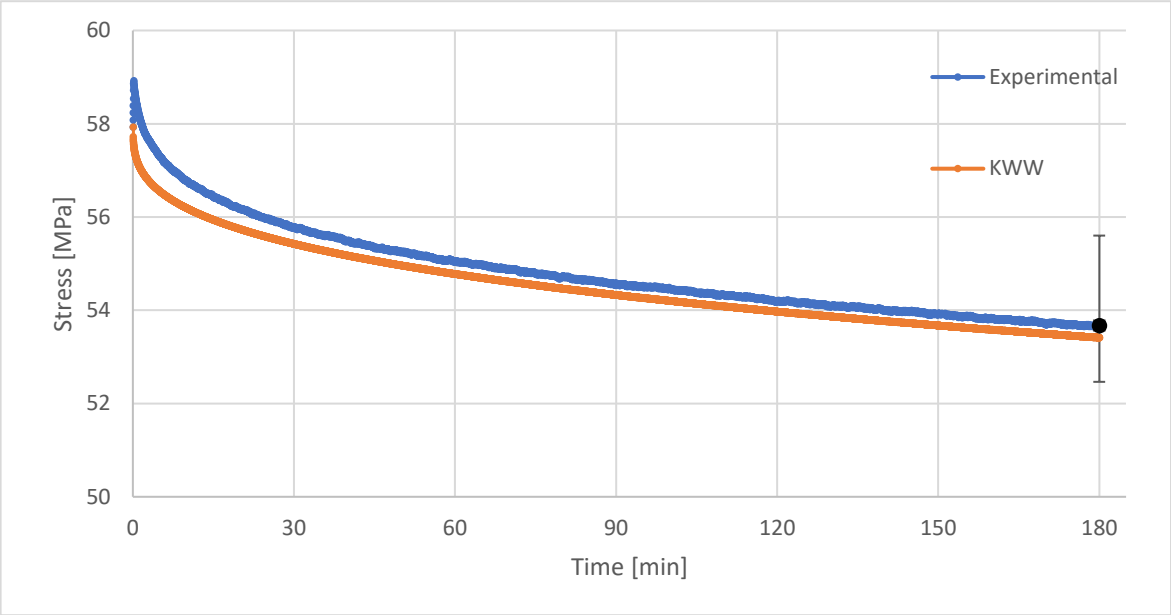


Figure 20 - Experimental and fitted KWW curves for stress relaxation.

From the figure above, it is possible to conclude that the two curves have very little deviation. For t=180 min the experimental stress was of around 53.7 MPa while the predicted value was of 53.4 MPa. Since not only the predicted value is within the limits delimited by the maximum and minimum values obtained for the experimental data, but also that the relative error is inferior to 0.5%, it is possible to conclude that the KWW model is a suitable model to predict the behavior of the adhesive throughout stress relaxations tests, and it is possible to confirm that the material is in fact linear viscoelastic. These results are the consequence of two mechanisms: physical and chemical phenomena. The physical phenomena is characterized by molecular rearrangements and the chemical phenomena by chain scission, crosslink scission or crosslink formation [6].
Table 5 summarizes the KWW parameters and the respective relative error in regards to the experimental results.

*Table 5 - Parameters of KWW for stress relaxation.*

| Initial bending stress [MPa] | β | τ | Bending stress after 180 min [mm] | | |
|---|---|---|---|---|---|
| | | | Experimental value | KWW value | Error [%] |
| 19,85 | 0,278 | 6,74E+07 | 18,53 | 19,30 | 4,16 |
| 40,44 | 0,332 | 4,59E+05 | 38,09 | 38,23 | 0,34 |
| 58,42 | 0,339 | 2,97E+05 | 54,27 | 53,87 | 0,74 |
| 63,34 | 0,352 | 1,80E+05 | 58,20 | 58,01 | 0,33 |

From the table it is possible to observe that the error is of less than 5% for all conditions which proves the viability of the model to predict the viscoelastic behavior.
In Figure 21 the average normalized creep curves (obtained by dividing the displacement at each moment by the initial one) are represented for a test time of 180 minutes.

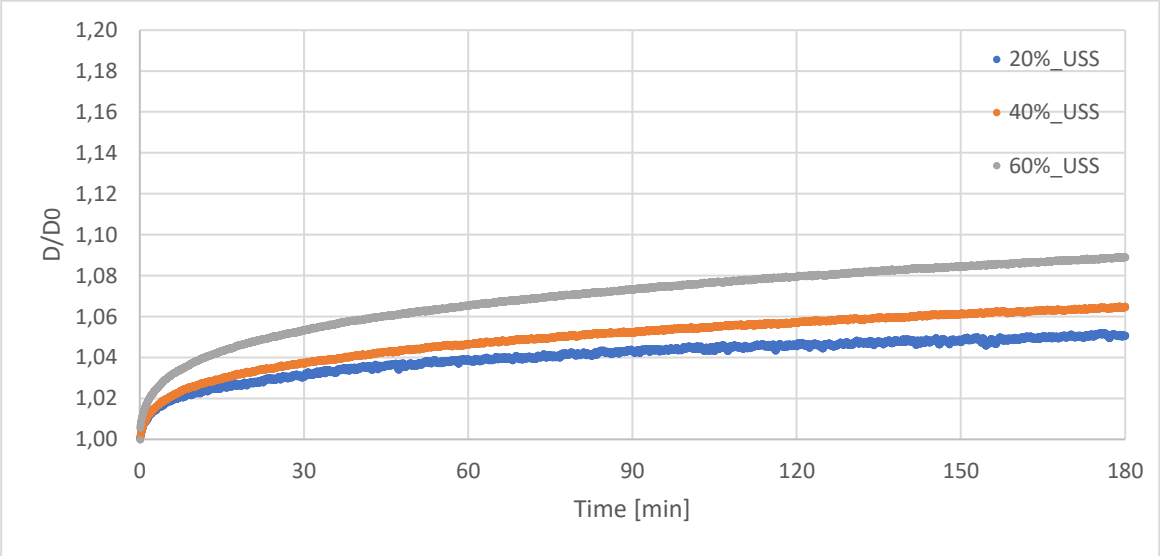


Figure 21 - Average normalized creep curves for different percentages of USS.

For all the curves represented it is possible to observe a very high initial increase in the displacement followed by a less accentuated increase. It is possible to identify the primary and secondary creep regimens. The separation between regimens happens at approximately 30 minutes. There is also a clear tendency showing the displacement to increase with an increase in the initial stress applied, hence we can conclude that it is stress dependent. This is in agreement with literature where it was found that the creep behavior is stress dependent [6]. Regarding the curve subjected to 20% of the ultimate stress it is possible to observe a lot more oscillations that for the others. This might be explained by the fact that since the applied load is small it is more susceptible to be influenced by outside noise and support vibrations.

The values of the curve in which the initial tension is 60% of the ultimate stress, an initial displacement around 5.3% can be observed while in the rest of the test the increase is around 3.4%. On the other hand, for the curve where the initial stress is of 20% of the ultimate stress, an initial displacement of around 3% can be observed while in the rest of the test the increase is of 2%.

In Figure 22 two curves are represented for creep tests. The curve obtained by the average experimental data for 50% of the ultimate stress strength, as well as the maximum and minimum values obtained for the final instant, and the theoretical data obtained by fitting the Findley model.

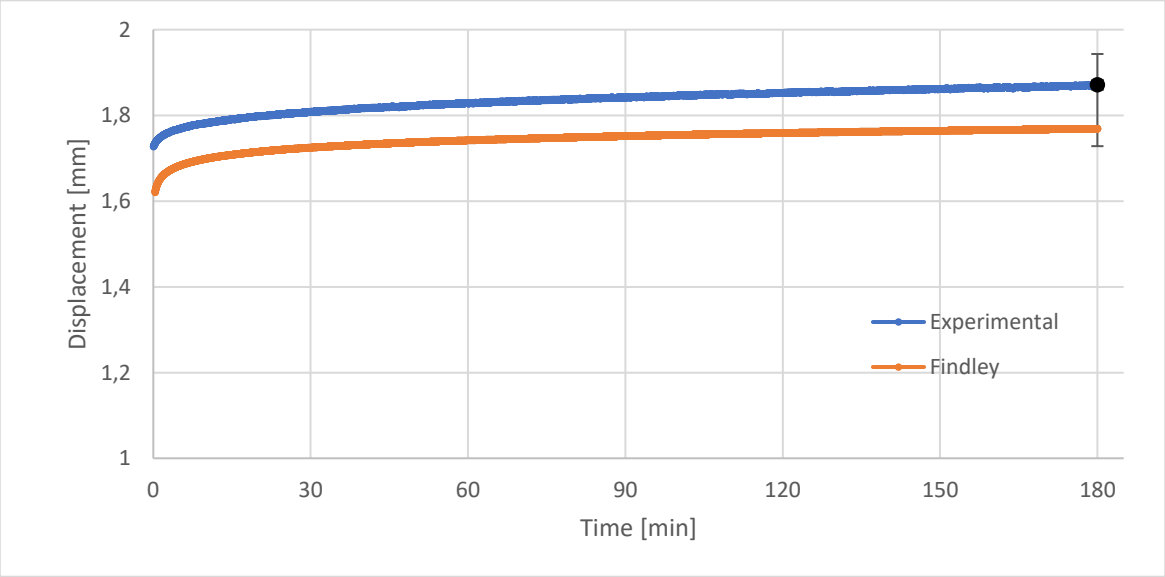


*Figure 22 - Experimental and fitted Findley curves for creep behavior.*

From the figure above it is observed that the Findley model can be used to predict the behavior of the adhesive for creep tests since it has a small deviation and as shown for t= 180 min the predicted value falls inside the range obtained for the experimental data. The relative error for the final instant is of around 5.4%.

For creep results, as the displacement increases the geometry of the walls is altered and a competition between bending and buckling of cell walls occurs [6].

Table 6 summarizes the Findley parameters and the respective relative error in regards to the experimental results.

*Table 6 - Parameters of Findley for creep.*

| **Bending stress [MPa]** | **$\varepsilon_0$** | **A** | **n** | **Displacement after 180 min [mm]** | | |
|---|---|---|---|---|---|---|
| | | | | **Exp. value** | **Findley value** | **Error [%]** |
| *19,85* | *0,4426* | *0,3171* | *0,0193* | *0,823* | *0,822* | *0,11* |
| *40,44* | *0,6736* | *0,6574* | *0,0233* | *1,492* | *1,489* | *0,22* |
| *58,42* | *0,7524* | *0,8082* | *0,0247* | *1,871* | *1,769* | *5,44* |
| *63,34* | *0,8406* | *0,9630* | *0,0263* | *2,076* | *2,070* | *0,29* |

From the table it is possible to conclude that the error is of less than 6% for all conditions which proves the viability of the model to predict creep behavior.

In order to evaluate the behavior of the physical properties (apparent density and apparent porosity) adhesive specimens were immersed in water and exposed to the temperatures of 20, 40 and 80ºC. In Figure 23 the apparent porosity is plotted in regard to time.

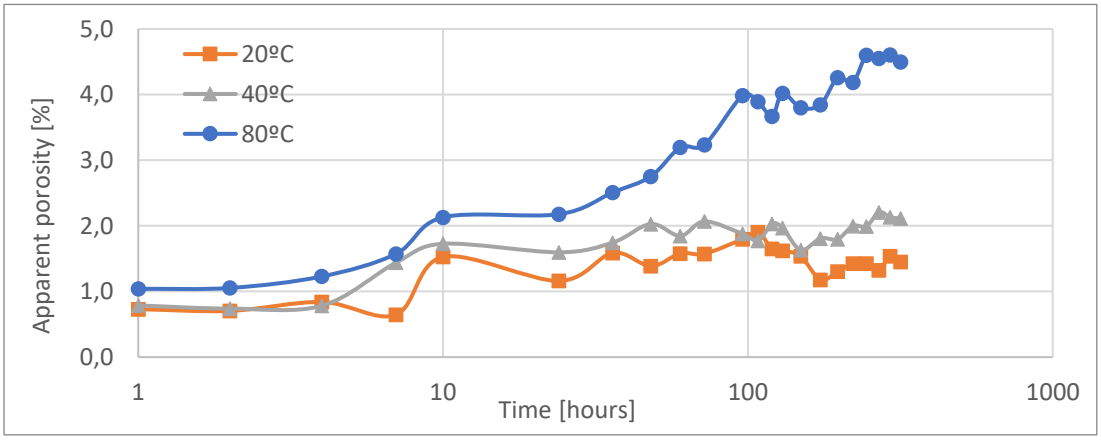


Figure 23 - Variation of apparent porosity with time for different temperatures.

From the figure it is possible to conclude that the maximum apparent porosity is achieved after ~300 hours with around 4.6% of apparent porosity for the specimens immersed in water and kept at 80ºC, as in compliance with the Standard ASTM C 20 [70]. So, these will be the environmental conditions that the bulk adhesive and the T-joints will be subjected to before testing them in order to compare them with the control group. It is also worth noting that the maximum apparent porosity seems to stabilize sooner and with a considerably lower apparent porosity for lower temperatures.

The final apparent porosity of the specimens kept at 80ºC is 4.5% whereas for 40ºC it is of 2.1% and for 20ºC of 1.5% accordingly. Thus, the variation in porosity when comparing the specimens kept at 20ºC and 40ºC is small especially when considering the difference to the ones kept at 80ºC.

Using similar analysis, the variation of the bulk density with the time is shown in Figure 24.

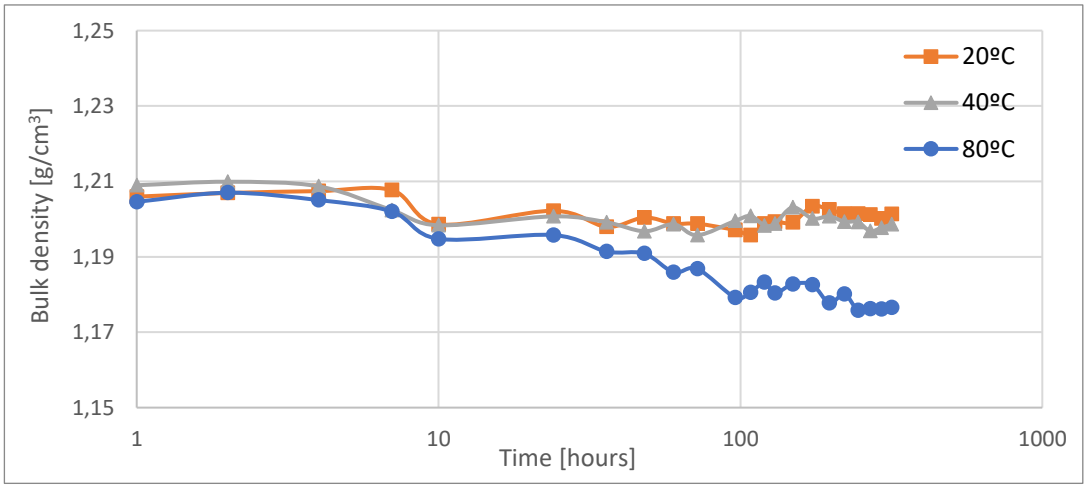


Figure 24 - Variation of bulk density with time for different temperatures.

From this behavior it can be observed that the decrease in density is much more accentuated for the specimens kept at 80ºC than for the other ones where the drop in density wasn't as noticeable.

The final bulk density (considering that water enters the open pores) of the specimens kept at 80ºC is of 1.17 g/cm³ whereas for 40ºC and 20ºC it is of ~1.2 g/cm³. As it happened for the apparent porosity the variation for the specimens kept at 80ºC is much more noticeable than the ones kept at 20ºC and 40ºC.

This non-linear variation of the apparent porosity and density with temperature is likely due to the viscosity profile of the adhesive where the viscosity doesn't vary linearly with the temperature but logarithmically.

In Figure 25 the flexural stress curves for the two types of specimens (control and aged) are represented.

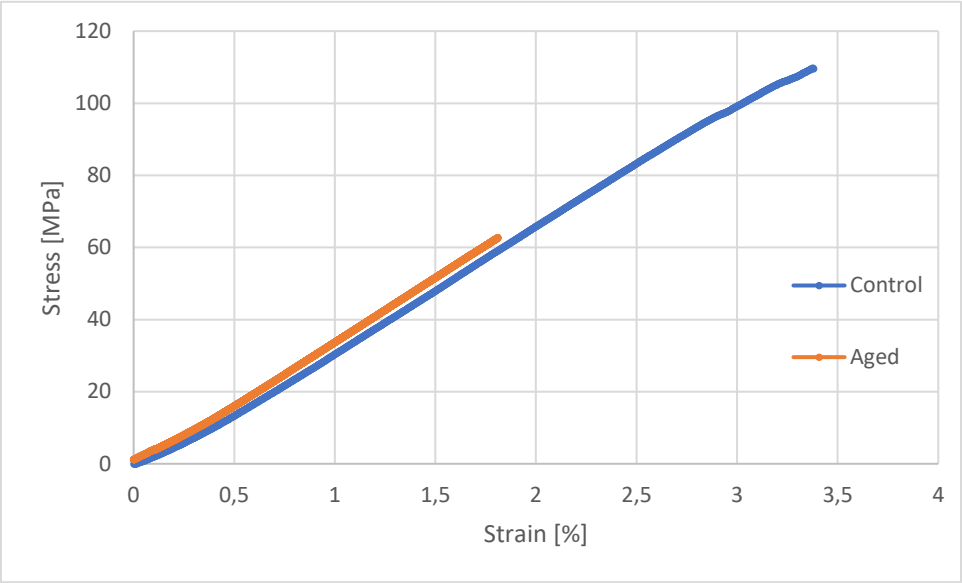


Figure 25 – Flexural stress curves for control and aged specimens.

From the figure it is observed a clear decline in the stress and the strain that the aged specimens can withstand before failure when compared with the control group. While the control group had an ultimate stress strength of around 104 MPa and a maximum deformation of around 3.2% the aged specimens had an ultimate stress strength around 68 MPa and a maximum deformation of around 1.9%. This corresponds to an ultimate stress reduction of 35% and a maximum deformation reduction of 40%. However little impact can be seen in the Elastic Modulus. This is in agreement with literature that states that the adhesive is highly affected by moisture and temperature resulting in a reduction of the mechanical properties [3].

In Figure 26 the average normalized stress relaxation curves (obtained by dividing the stress at each moment by the initial one) for 60% of the USS for the two types of specimens (control and aged) are represented for a test time of 180 minutes.

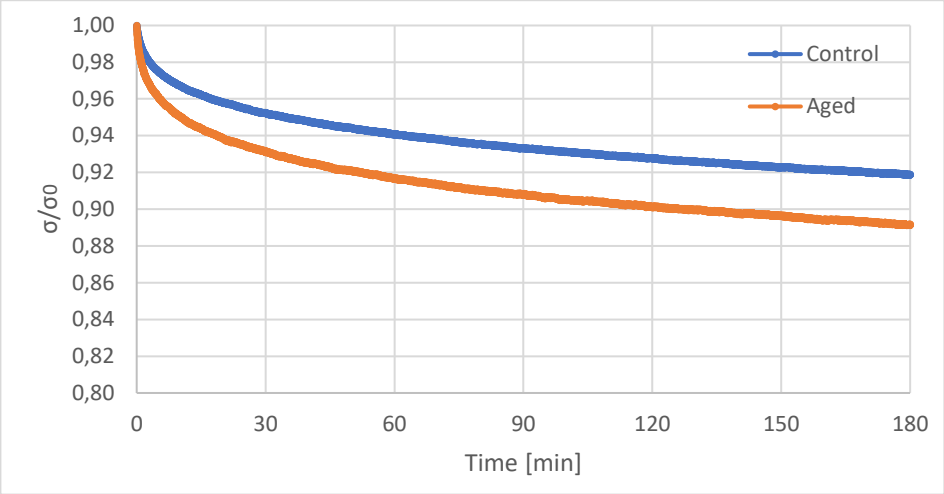


Figure 26 – Normalized stress relaxation curves for control and aged specimens.

From the figure it can be seen that when t=180 min the normalized stress for the control specimens is of around 0.92 while for the aged specimens the normalized stress is of around 0.89. This shows that there was an increase in stress relaxation. This is supported by the literature that states that for a low moisture content there is a positive influence in stress relaxation due to plasticization [83].

In Figure 27 the average normalized creep curves (obtained by dividing the displacement at each moment by the initial one) for 60% pf the USS for the two types of specimens (control and aged) are represented for a test time of 180 minutes.

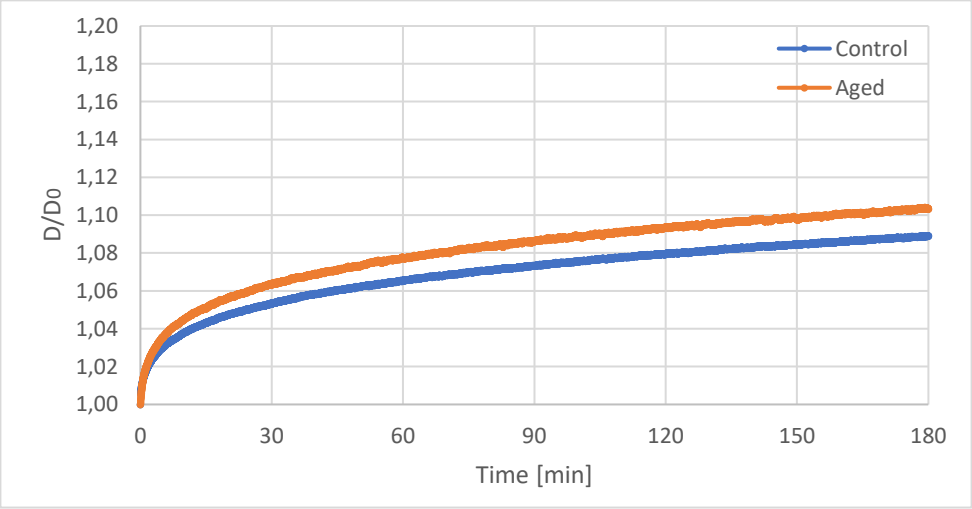


Figure 27 – Normalized creep curves for control and aged specimens.

From the behavior it is observed that when t= 180 min the normalized displacement for the control specimens is of around 1.09 while for the aged specimens the normalized displacement is of above 1.1. This shows that, as seen for the stress relaxation, there was also an increase in creep behavior. This is related to the fact that the same that the mechanisms that influence creep are the same mechanisms that influence stress relaxation (cell wall bending and post-buckling deformation) so, the same viscous phenomena that occurs at cell walls that cause the stress decrease in stress relaxation will also increase the creep displacement [6].

## 4.2 Stiffener Pull-Off Test

In Figure 28 the results obtained for the Stiffener pull-off tests (SPOT) are represented.

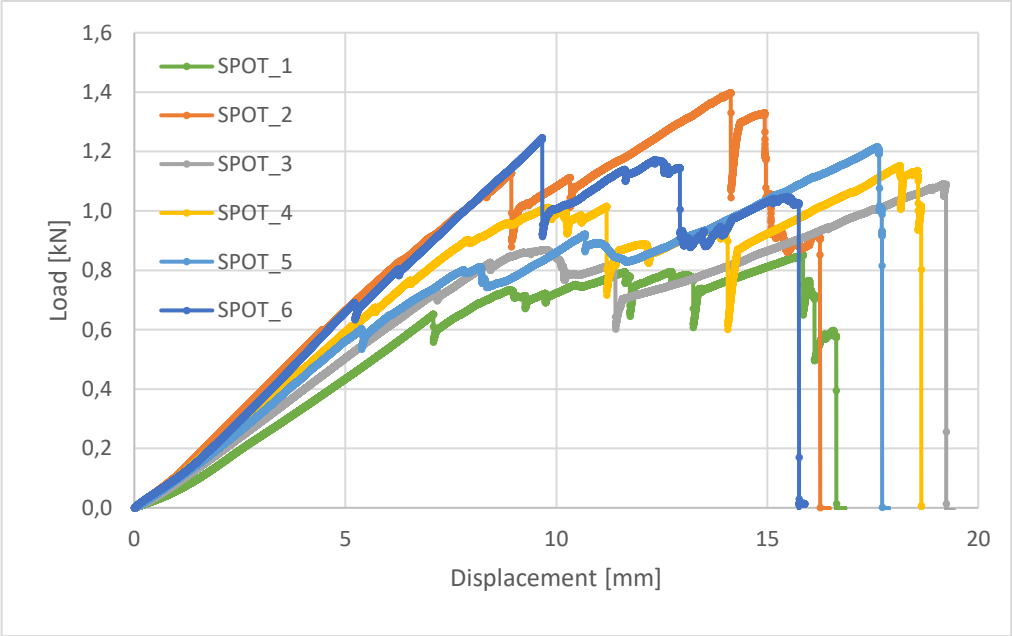


Figure 28 - Load-displacement curves for all tested T-joints.

From the figure it was possible to verify a considerable discrepancy between results so a surface examination was done to analyze whether the T-joints failed prematurely due to defects, in particularly the presence of voids with reduction of adhesive area. From this analysis the SPOT_1, SPOT_3 and SPOT_5 were excluded. In Figure 29 it is illustrated the usual type of defect encountered in the bondline that led to premature failure.

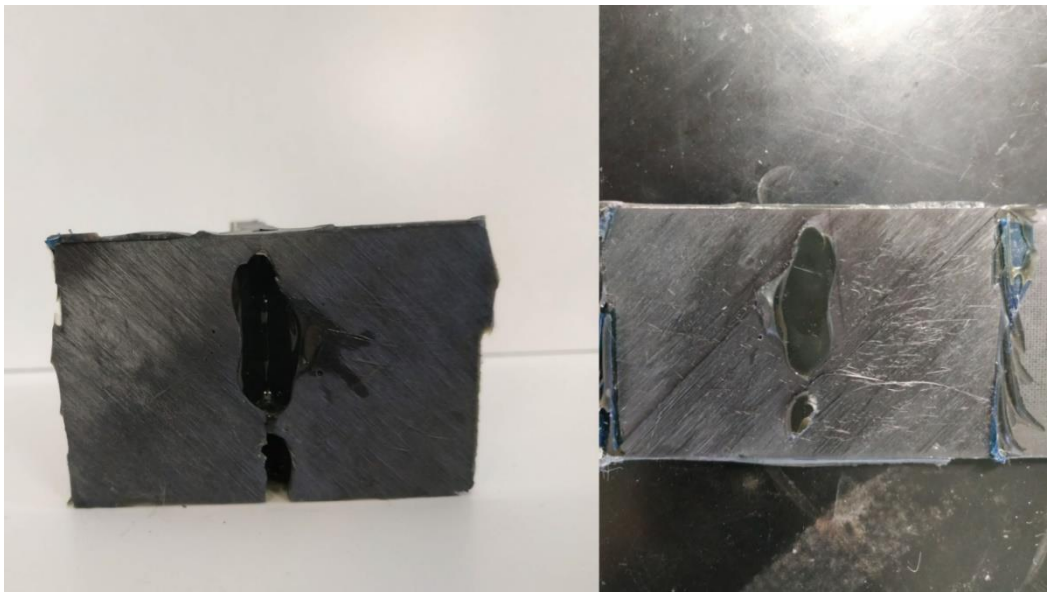

*Figure 29 – Typical defects found in bondline. Absence of adhesive in some parts of bonded joint.*

From the figure it can be seen a part on both the skin and stiffener where adhesion didn't occur which led to premature failure of the bonded joint.

Having excluded the defected specimens in Figure 30 it is possible to observe the behavior obtained for the valid specimens.

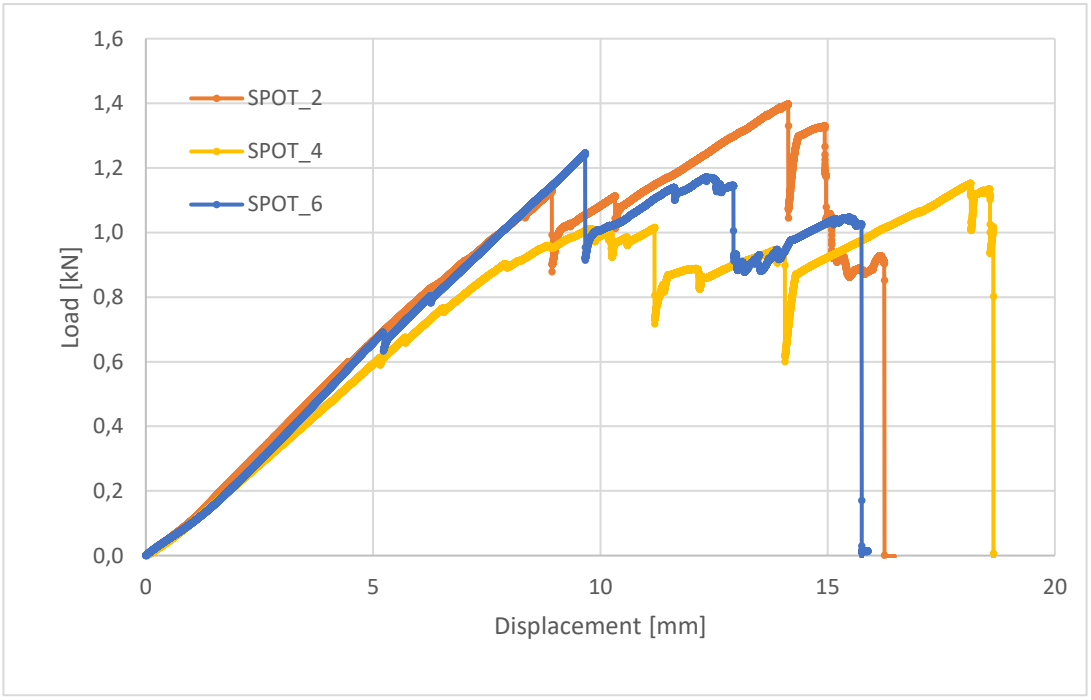


*Figure 30 - Representative load-displacement curves for T-joints.*

From the figure above it is shown that the T-joints have a maximum load of around 1.26 kN and that the maximum displacement is of around 16.8 mm. Additionally it is also shown that the first significative failure occurs for a displacement of around 8.9 mm. Since one of the major disadvantages usually mentioned in literature when talking about CFRP is the very brittle behavior and abrupt catastrophic failure, and since in this case the first failure occurs at around 9 mm while the final failure occurs at around 17 mm we can conclude that this type of CFRP T-joints negates that effect [84]. In Table 7 a comparison is made between the results obtained for the average of the T-joints, as well as the standard deviation, and the values reported in literature [42]. The results show the maximum load sustained, the displacement at maximum load and the maximum displacement.

Table 7 - Comparison between experimental and literature reported values for T-joints.

| | $P_{max}$ [N] | $\delta_{Pmax}$ [mm] | $\delta_{max}$ [mm] |
|---|---|---|---|
| Experimental | 1260±125 | 14.0±4.4 | 16.8±1.7 |
| Reported in literature [39] | 1064 | 14.2 | 14.2 |

By the analysis of the load-displacement figure and the values obtained in the Table above we can conclude that the results (Load and displacement) obtained for the T-joints are in agreement (similar order) with the literature and that the CFRP T-joints are a viable option for aeronautical applications as a whole, and more specifically for primary structures since they can sustain considerable load before failure and support considerable displacement giving the chance to be replaced before failure. A peak analysis is done below.
In Figure 31 the SPOT_6 Load-Displacement curve is represented with its characteristic behavior. Four points are marked in the figure that are directly linked to the four images in Figure 32 showing the failure sequence observed in all specimens.

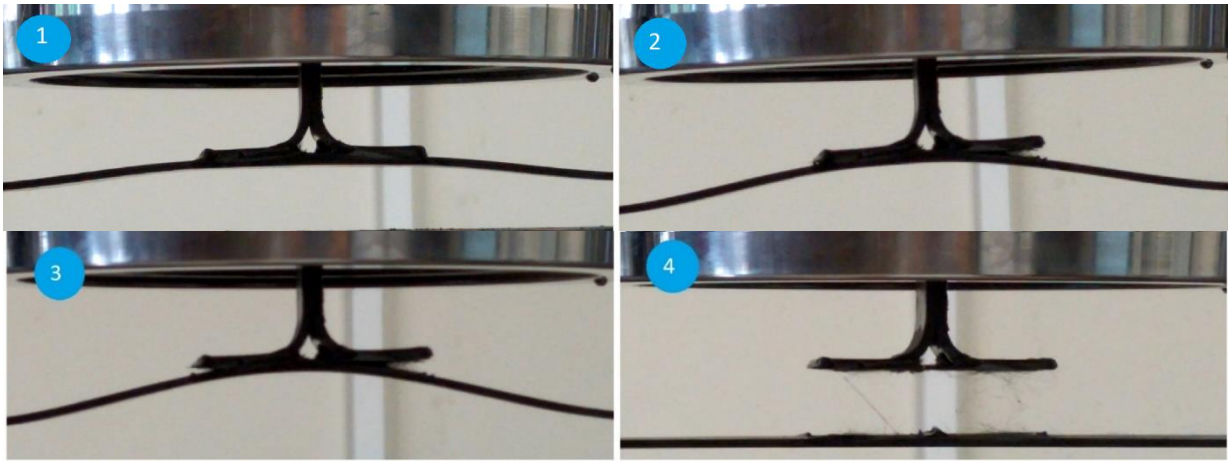


*Figure 32 - Failure sequence observed for all T-joints.*

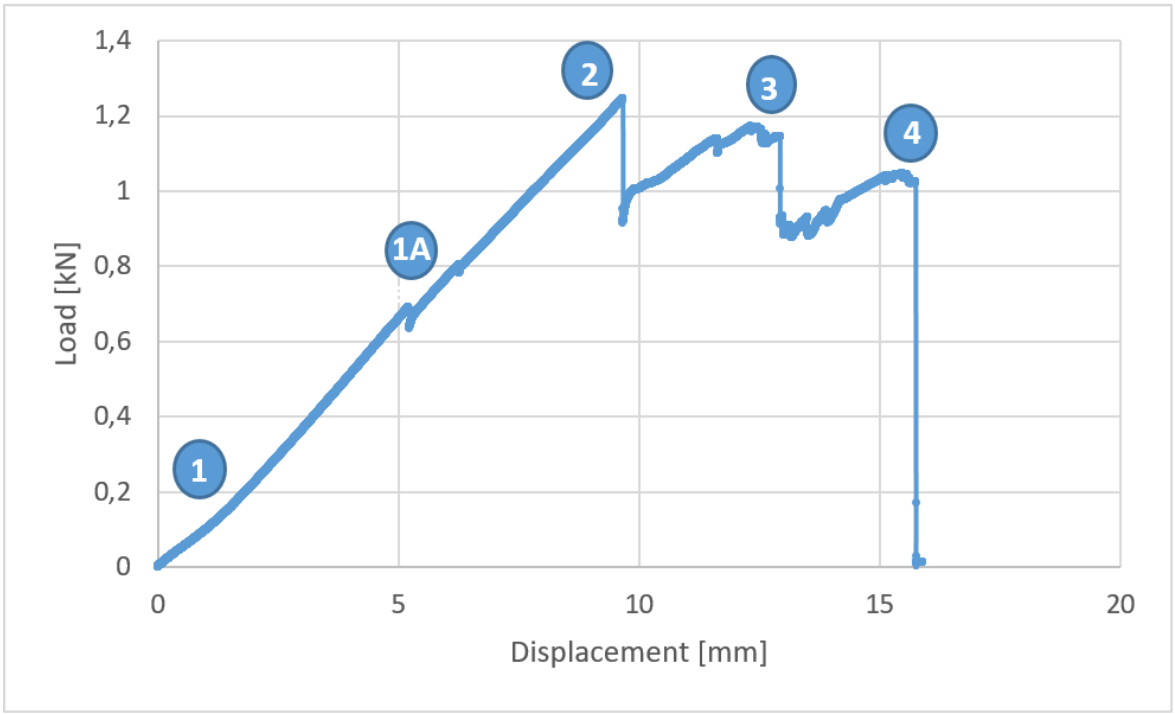


*Figure 31 - SPOT_6 Load-displacement curve.*

From the analyzes of both figures above it can be observed that the usual failure sequence:

(1) Starts in the toe region until the linear region;

(1A) Breakage of small deposits of adhesive on the edge of skin and stiffener;

(2) First detachment in one of the tips of the T-joint;

(3) Followed by the second detachment of the other tip;

(4) Catastrophic rupture with complete separation of the stiffener from the skin.

This failure sequence is in agreement with the previous studies in the group [42] and can be justified as follows: first there is only Mode I since the applied load is completely perpendicular to the T-joint hence only tensile opening exists. As the skin starts to bend Mode II appears. Even though the shear stress is considerably smaller than the tensile one it cannot be overlooked because it has an impact on the propagation of the failure from the tip of the T-joint towards the middle. The same happens on the other side of the T-joint. When both failure propagations meet disbound occurs.
In Figure 33 it is shown the skin and stiffener post-failure.

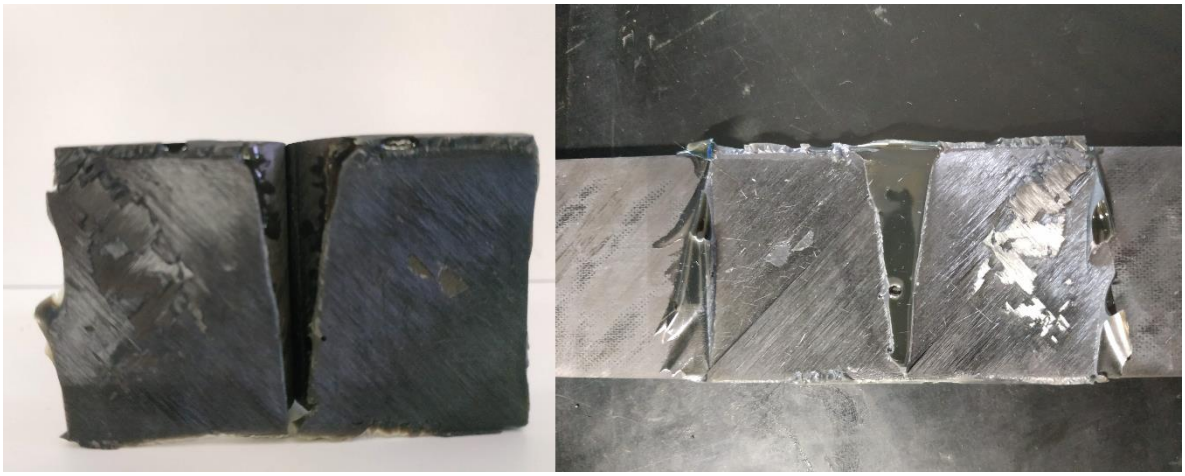

*Figure 33 - Feature surface post-failure of the skin and stiffener.*

From the Figure it is possible to conclude that the failure mode was light-fiber-tear failure, following the designations presented in the Standard ASTM D5573-99 [36]. This was the failure mode encountered in all tested specimens.

For the specimens that have undergone environmental ageing (~300h at 80ºC immersed in water) the results are presented below. In Figure 34 the results obtained from the Stiffener pull-off tests for the aged specimens are represented.

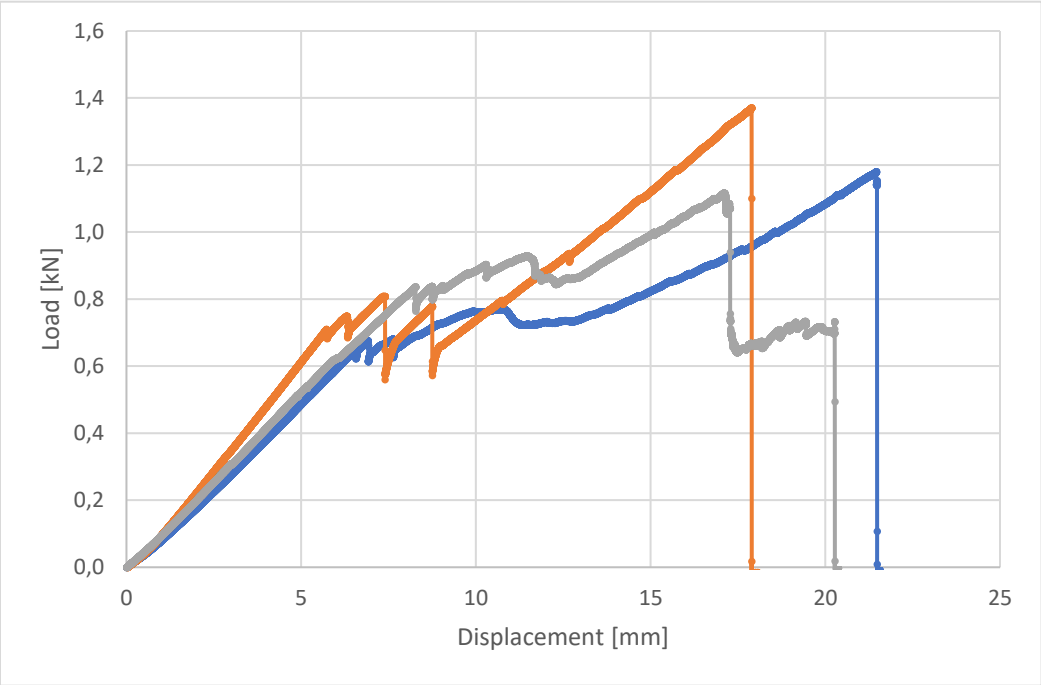


Figure 34 - Load-displacement curves for aged T-joints.

From the figure it is observed that the T-joints had 3 drops in load that correspond to the same failure sequence mentioned for the control group and the same failure mode. However, it is worth mentioning that even after being dried for 24 hours at room temperature, the adhesive surface still presented moisture. The fact that the failure mode didn't shift from light-fiber-tear to interfacial failure, which is the region usually more degraded by hydrothermal conditions, seems to tells us that this is a tendency more pronounced with an increase in temperature that leads us to believe that the temperature chosen wasn't high enough to cause the weakening of the adhesive-adherend interface to the point where a change in failure mode occurred [85].

In Table 8 a summary is made in order to compare the loads and the displacements during the failure mode of the two types of specimens. The values represented are the average and the corresponding standard deviation.

Table 8 - Comparison of load and displacement for each failure for control and aged specimens.

| Specimens | First detachment | | Second detachment | | Catastrophic rupture | |
|---|---|---|---|---|---|---|
| | $P_l$ [kN] | δ [mm] | $P_l$ [kN] | δ [mm] | $P_l$ [kN] | δ [mm] |
| **Control** | 1.13±0.12 | 9.91±1.16 | 1.16±0.23 | 13.67±0.70 | 1.02±0.11 | 16.86±1.54 |
| **Aged** | 0.80±0.13 | 8.99±2.30 | 0.87±0.19 | 12.32±4.42 | 1.07±0.34 | 19.87±1.85 |

From the summary above it is observed that for the first and second failure the control group has higher values which is expected since it wasn't subjected to environmental degradation. However, for the final failure it was found that both the load and displacement of the T-joints with environmental degradation presented higher values. Being subjected to a higher temperature and moisture leads to an increase in ductility which is why the specimens that suffered degradation presented a higher displacement. This is usually accompanied by a reduction in ultimate load which is also verified [3]. However, this reduction is hardly noticeable since CFRP have shown significantly less moisture absorption than thermosets. The properties most affected tend to be matrix-dominated properties. This supports why the ultimate load had little variation by hydrothermal conditions but the displacement had considerable variation since the ultimate load is more reliant on fiber properties while the displacement is more reliant on matrix properties [83], [86].

In Figure 35 the normalized stress relaxation curves for the two types are represented.

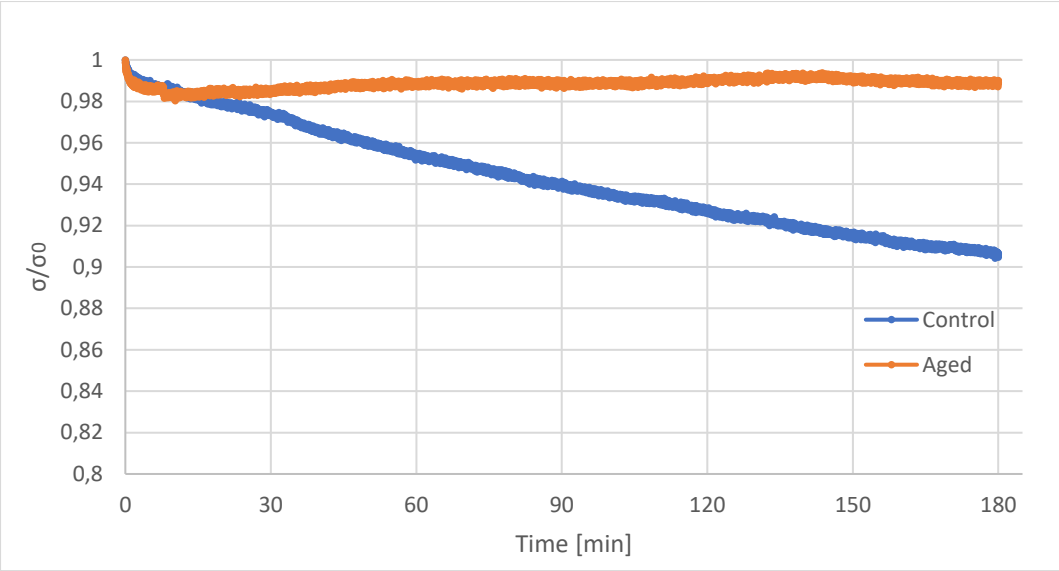


*Figure 35 - Normalized relaxation stress curves for control and aged T-joints.*

From the figure it can be observed that the control group has the usual trend reported for polymers however, the specimen that suffered environmental ageing has only a slight initial drop and then remains practically constant the rest of the test. When comparing the final stress with the initial for the control specimen the decrease was of around 9% while for the aged specimen the decrease was of around 1%. Study done by LaPlante *et al.* [87] states that for hydrothermal aging there are two competing mechanisms that define the behavior of the specimen. When there is a low moisture content due to plasticization the material can relax more easily. However, after moisture exceeds the threshold the water molecules start to impede stress relaxation. Since for the bulk adhesive the aged specimens showed a better stress relaxation response than the control specimens while for the T-joint it is possible to observe not only the opposite but also a huge negative impact for the aged specimen when subjected to stress relaxation we are led to conclude that the hydrothermal effects are very complex and that the whole system must be taken into account since each of the components (adherends, adhesive, interphase regions) can strongly affect the behavior of the joint [30]. However, further tests should be done in order to verify this tendency and to properly characterize the mechanisms that influence the viscoelastic behavior of the T-joint.

# Chapter 5 – Closing Remarks

In this chapter, the main findings collected over the dissertation are summarized. They are presented in the same order as they appear in the discussion of the results, in order to be gradually consistent. Suggestions for future work are also presented.

## 5.1 Final Conclusions

The objectives defined in Chapter 1 were accomplished and the following conclusions can be drawn:

- A fabrication method that minimized the appearance of voids in the adhesive was found.
- The adhesive mechanical properties are strain-rate sensitive.
- The adhesive has linear viscoelastic properties so stress relaxation and creep behavior can be predicted.
- Stress relaxation and creep behavior can be accurately modeled with the KWW and Findley model respectively. The error associated with the former was inferior to 0.5% while for the latter it was of 5.4%.
- The adhesive has a non-linear variation of the apparent porosity and density with temperature.
- There is a clear degradation in the mechanical properties of the adhesive when subjected to hydrothermal conditions.
- Plasticization is shown to improve the viscoelastic behavior of the adhesive for bulk testing.
- CFRP T-joints presents a non-catastrophic rupture, but a failure mode characterized by successive steps: First detachment in one of the tips; Second detachment of the other tip; Catastrophic rupture with complete separation.
- For T-joints there was a clear impact on the mechanical performance when subjected to hydrothermal conditions.

## 5.2 Future Work

Considering the results obtained for the stress relaxation of the T-joint further research into the viscoelastic behavior and hydrothermal effects is needed to have a better understanding how each component influences the performance of the T-joint in order to be able to characterize its behavior and with this build trust in CFRP as primary structures taking an even greater leap in regards to use of composites in aeronautical structures. Research on optimizing T-joints by using mixed adhesives would also allow an increment in the mechanical properties with no change in weight by creating a more even stress distribution. The lack of research on the viscoelastic behavior of adhesive joints using mixed adhesives shows that this area is still unexplored.

The complexity of mechanisms involved in viscoelastic behavior, environmental degradation and mixed adhesives makes it very hard to isolate and evaluate the impact of each mechanism individually so FEM tools could be seen as an option to help properly evaluate the impact of each individual mechanism.

# References


[1] T. Kruse, “Bonding of CFRP primary aerospace structures,” no. June, 2013.

[2] Institution of Structural Engineers (ISE), “A guide to the structural use of adhesives,” no. January, p. 51, 1999.

[3] S. Budhe, M. D. Banea, S. de Barros, and L. F. M. da Silva, “An updated review of adhesively bonded joints in composite materials,” *Int. J. Adhes. Adhes.*, vol. 72, no. October 2016, pp. 30–42, 2017.

[4] H. F. Brinson and L. C. Brinson, *Polymer Engineering Science and Viscoelasticity: An Introduction*. 2008.

[5] A. Ilioni, C. Badulescu, N. Carrere, P. Davies, and D. Thévenet, “A viscoelastic-viscoplastic model to describe creep and strain rate effects on the mechanical behaviour of adhesively-bonded assemblies,” *Int. J. Adhes. Adhes.*, vol. 82, no. December 2017, pp. 184–195, 2018.

[6] P. N. B. Reis, M. P. Silva, P. Santos, J. M. Parente, and A. Bezazi, “Viscoelastic behaviour of composites with epoxy matrix filled by cork powder,” *Compos. Struct.*, vol. 234, no. November 2019, p. 111669, 2020.

[7] E. Barbero, *Introduction to composite materials design*. CRC Press, 2017.

[8] K. Chawla, *Composite materials*. Springer International Publishing, 2011.

[9] E. Barbero, *Finite element analysis of composite materials using ANSYS*. CRC Press, 2007.

[10] A. P. Mouritz, “Fibre–polymer composites for aerospace structures and engines,” in *Introduction to Aerospace Materials*, no. chapter 15, 2012, pp. 338–393.

[11] H. M.Flower, *High performance materials in aerospace*. 1995.

[12] J. Hale, “Boeing 787 from the ground up,” *Adv. Mech. Eng.*, vol. 11, no. 3, 2006.

[13] J. Bachmann, C. Hidalgo, and S. Bricout, “Environmental analysis of innovative sustainable composites with potential use in aviation sector—A life cycle assessment review,” *Sci. China Technol. Sci.*, vol. 60, no. 9, pp. 1301–1317, 2017.

[14] X. Ma, K. Bian, J. yun Lu, and K. Xiong, “Experimental research on detection for interface debond of CFRP T-joints under tensile load,” *Compos. Struct.*, vol. 158, pp. 359–368, 2016.

[15] L. Burns, A. P. Mouritz, D. Pook, and S. Feih, “Strengthening of composite T-joints using novel ply design approaches,” *Compos. Part B Eng.*, vol. 88, pp. 73–84, 2016.

[16] T. H. Ooijevaar, M. D. Rogge, R. Loendersloot, L. L. Warnet, R. Akkerman, and T. Tinga, “Nonlinear dynamic behavior of an impact damaged composite skin-stiffener structure,” *J. Sound Vib.*, vol. 353, pp. 243–258, 2015.

[17] Z. X. Wang, Y. Q. Wang, G. X. Zhang, and Y. J. Shi, “Tests and parametric analysis of aluminum alloy bolted joints of different material types,” *Constr. Build. Mater.*, vol. 185, pp. 589–599, 2018.

[18] Y. Zhao, L. Zhou, Q. Wang, K. Yan, and J. Zou, “Defects and tensile properties of 6013 aluminum alloy T-joints by friction stir welding,” *Mater. Des.*, vol. 57, pp. 146–155, 2014.

[19] S. Meco, S. Ganguly, S. Williams, and N. McPherson, “Design of laser welding applied to T joints between steel and aluminium,” *J. Mater. Process. Technol.*, vol. 268, no. January, pp. 132–139, 2019.

[20] X. Xiong, P. Zhao, R. Ren, Z. Zhang, X. Cui, and S. Ji, “Enhanced resistance-welding hybrid joints of titanium alloy/thermoplastic composites using a carbon-nanotube lamina,” *Diam. Relat. Mater.*, vol. 101, no. September 2019, p. 107611, 2020.

[21] X. Liu, H. Cui, S. Zhang, H. Liu, G. Liu, and S. Li, “Experimental and numerical investigations on fatigue behavior of aluminum alloy 7050-T7451 single lap four-bolted joints,” *J. Mater. Sci. Technol.*, vol. 34, no. 7, pp. 1205–1213, 2018.

[22] C. V. Chris Worrall, Kellar Ewen, “Joining of Fibre-Reinforced Polymer Composites.”

[23] M. Yari, “Galvanic Corrosion of Metals Connected to Carbon Fiber Reinforced

Polymers," 2017. [Online]. Available: https://www.corrosionpedia.com/galvanic-corrosion-of-metals-connected-to-carbon-fiber-reinforced-polymers/2/1556. [Accessed: 16-Aug-2020].

[24] H. Mahfuz, P. Majumdar, M. Saha, F. Shamery, and S. Jeelani, "Integral manufacturing of composite skin-stringer assembly and their stability analyses," *Appl. Compos. Mater.*, vol. 11, no. 3, pp. 155–171, 2004.

[25] M. A. S. Carneiro and R. D. S. G. Campilho, "Analysis of adhesively-bonded T-joints by experimentation and cohesive zone models," *J. Adhes. Sci. Technol.*, vol. 31, no. 18, pp. 1998–2014, 2017.

[26] G. Scarselli, C. Corcione, F. Nicassio, and A. Maffezzoli, "Adhesive joints with improved mechanical properties for aerospace applications," *Int. J. Adhes. Adhes.*, vol. 75, no. March, pp. 174–180, 2017.

[27] S. Ebnesajjad, *Handbook of adhesives and surface preparation*. Elsevier Inc., 2011.

[28] L. F. M. da Silva, A. Ochsner, and R. D. Adams, *Handbook of Adhesion Technology*. 2011.

[29] S. Ebnesajjad, *Adhesives technology handbook*. William Andrew Publishing, 2008.

[30] M. D. Banea and L. F. M. Da Silva, "Adhesively bonded joints in composite materials: An overview," *Proc. Inst. Mech. Eng. Part L J. Mater. Des. Appl.*, vol. 223, no. 1, pp. 1–18, 2009.

[31] R. Avendaño, R. J. C. Carbas, E. A. S. Marques, L. F. M. da Silva, and A. A. Fernandes, "Effect of temperature and strain rate on single lap joints with dissimilar lightweight adherends bonded with an acrylic adhesive," *Compos. Struct.*, vol. 152, pp. 34–44, 2016.

[32] G. H. Lim, M. Heidari-Rarani, K. Bodjona, K. P. Raju, V. Romanov, and L. Lessard, "Mechanical characterization of a flexible epoxy adhesive for the design of hybrid bonded-bolted joints," *Polym. Test.*, vol. 79, no. April, p. 106048, 2019.

[33] M. Nakanouchi, C. Sato, Y. Sekiguchi, K. Haraga, and H. Uno, "Development of application method for fabricating functionally graded adhesive joints by two-

component acrylic adhesives with different elastic moduli," *J. Adhes.*, vol. 95, no. 5–7, pp. 529–542, 2019.

[34] J. F. Durodola, "Functionally graded adhesive joints – A review and prospects," *Int. J. Adhes. Adhes.*, vol. 76, no. February, pp. 83–89, 2017.

[35] A. Pocius and D. A. Dillard, "Adhesion science and engineering - 1 'The mechanics of adhesion,'" no. 3, 2002.

[36] American Society for Testing and Materials, "ASTM D5573-99, Standard Practice for Classifying Failure Modes in Fiber-Reinforced-Plastic (FRP) Joints." ASTM International, 1999.

[37] J. B. Bai, C. H. Dong, J. J. Xiong, C. Y. Luo, and D. Chen, "Progressive damage behaviour of RTM-made composite T-joint under tensile loading," *Compos. Part B Eng.*, vol. 160, no. July 2018, pp. 488–497, 2019.

[38] E. Oterkus, C. Diyaroglu, D. De Meo, and G. Allegri, *Marine applications of advanced fibre-reinforced composites*. 2016.

[39] C. Branco, *Mecânica dos materiais*. Fundação Calouste Gulbenkian, 1998.

[40] R. P. Romero and Á. L. Ramírez, "Analysis of rubber adhesive - FE simulation of damage propagation over rubber adhesive under fatigue in mixed-mode loading," 2014.

[41] S. Akpinar, M. D. Aydin, and A. Özel, "A study on 3-D stress distributions in the bi-adhesively bonded T-joints," *Appl. Math. Model.*, vol. 37, no. 24, pp. 10220–10230, 2013.

[42] J. V. Cardoso, P. V. Gamboa, and A. P. Silva, "Effect of surface pre-treatment on the behaviour of adhesively-bonded CFRP T-joints," *Eng. Fail. Anal.*, vol. 104, no. May, pp. 1188–1202, 2019.

[43] Google, "Google Scholar," *T-joints*. [Online]. Available: https://scholar.google.com. [Accessed: 27-Mar-2020].

[44] M. K. Apalak and R. Davies, "Analysis and design of adhesively bonded corner joints,"

*Int. J. Adhes. Adhes.*, vol. 13, no. 4, pp. 219–235, 1993.

[45] S. M. R. Khalili and A. Ghaznavi, "Numerical analysis of adhesively bonded T-joints with structural sandwiches and study of design parameters," *Int. J. Adhes. Adhes.*, vol. 31, no. 5, pp. 347–356, 2011.

[46] X. Hou, X. Yang, L. Cui, and G. Zhou, "Influences of joint geometry on defects and mechanical properties of friction stir welded AA6061-T4 T-joints," *Mater. Des.*, vol. 53, pp. 106–117, 2014.

[47] F. Dharmawan, R. S. Thomson, H. Li, I. Herszberg, and E. Gellert, "Geometry and damage effects in a composite marine T-joint," *Compos. Struct.*, vol. 66, no. 1–4, pp. 181–187, 2004.

[48] L. A. Burns, A. P. Mouritz, D. Pook, and S. Feih, "Strength improvement to composite T-joints under bending through bio-inspired design," *Compos. Part A Appl. Sci. Manuf.*, vol. 43, no. 11, pp. 1971–1980, 2012.

[49] R. A. Shenoi and F. L. M. Violette, "A Study of Structural Composite Tee Joints in Small Boats," *J. Compos. Mater.*, vol. 24, no. 6, pp. 644–666, 1990.

[50] E. Theotokoglou, "Strength of Composite T-Joints under Pull-Out Loads," *Reinf. Plast. Compos.*, vol. 9, no. 2, pp. 183–205, 1997.

[51] W. Li, L. Blunt, and K. J. Stout, "Analysis and design of adhesive-bonded tee joints," *Int. J. Adhes. Adhes.*, vol. 17, no. 4, pp. 303–311, 1997.

[52] A. Kesavan, S. John, and I. Herszberg, "Strain-based structural health monitoring of complex composite structures," *Struct. Heal. Monit.*, vol. 7, no. 3, pp. 203–213, 2008.

[53] B. Whittingham, H. C. H. Li, I. Herszberg, and W. K. Chiu, "Disbond detection in adhesively bonded composite structures using vibration signatures," *Compos. Struct.*, vol. 75, no. 1–4, pp. 351–363, 2006.

[54] J. W. H. Yap, M. L. Scott, R. S. Thomson, and D. Hachenberg, "The analysis of skin-to-stiffener debonding in composite aerospace structures," *Compos. Struct.*, vol. 57, no. 1–4, pp. 425–435, 2002.

[55] J. I. R. Blake, R. A. Shenoi, J. House, and T. Turton, “Progressive damage analysis of tee joints with viscoelastic inserts,” *Compos. Part A Appl. Sci. Manuf.*, vol. 32, no. 5, pp. 641–653, 2001.

[56] S. Kumar and P. C. Pandey, *Behaviour of bi-adhesive joints*, vol. 24, no. 7. 2010.

[57] R. J. C. Carbas, L. F. M. Da Silva, M. L. Madureira, and G. W. Critchlow, “Modelling of functionally graded adhesive joints,” *J. Adhes.*, vol. 90, no. 8, pp. 698–716, 2014.

[58] M. D. Fitton and J. G. Broughton, “Variable modulus adhesives: An approach to optimised joint performance,” *Int. J. Adhes. Adhes.*, vol. 25, no. 4, pp. 329–336, 2005.

[59] Ş. Temiz, “Application of bi-adhesive in double-strap joints subjected to bending moment,” *J. Adhes. Sci. Technol.*, vol. 20, no. 14, pp. 1547–1560, 2006.

[60] N. Stein, P. Weißgraeber, and W. Becker, “Stress solution for functionally graded adhesive joints,” *Int. J. Solids Struct.*, vol. 97_98, pp. 300–311, 2016.

[61] V. V. S. Rao, K. Krishna Veni, and P. K. Sinha, “Behaviour of composite wing t-joints in hygrothermal environments,” *Aircr. Eng. Aerosp. Technol.*, vol. 76, no. 4, pp. 404–413, 2004.

[62] S. Kumari and P. K. Sinha, “Effects of Transverse Stitching and Hygrothermal Environment on Composite Wing T-Joints,” *J. Reinf. Plast. Compos.*, vol. 22, no. 18, pp. 1705–1728, 2003.

[63] CIT, “Datasheet HS 160 UD.” .

[64] Composite Materials (Italy) s.r.l., “EA451 Adhesive Film | Technical Data,” 2015.

[65] American Society for Testing and Materials, “ASTM D790-03, Standard test methods for flexural properties of un-reinforced and reinforced plastics and electrical insulating materials,” *Annu. B. ASTM Stand. Plast. (1), C177-D1600*, pp. 290–298, 2003.

[66] J. V. Cardoso, J. Nunes-Pereira, and A. P. Silva, “Fabrication of adhesively-bonded CFRP T-joints for stiffener pull-off tests,” *XVI Port. Conf. Fract.*, no. April, 2018.

[67] American Society for Testing and Materials, “ASTM D2991 - Standard Practice for

Testing Stress- Relaxation of Plastics."

[68] American Society for Testing and Materials, "ASTM D2990 - 17, Standard Test Methods for Tensile, Compressive, and Flexural Creep and Creep-Rupture of Plastics." 2017.

[69] P. N. B. Reis, M. P. Silva, P. Santos, J. M. Parente, S. Valvez, and A. Bezazi, "Mechanical performance of an optimized cork agglomerate core-glass fibre sandwich panel," *Compos. Struct.*, vol. 245, no. February, p. 112375, 2020.

[70] American Society for Testing and Materials, "ASTM C 20, Standard Test Methods for Apparent Porosity, Water Absorption, Apparent Specific Gravity, and Bulk Density of Burned Refractory Brick and Shapes by Boiling Water," *Methods*, vol. 93, no. April 1993, pp. 1–6, 2000.

[71] J. Bishopp, "Aerospace : A Pioneer in Structural Adhesive Bonding," 2005.

[72] E. A. de Sousa Marques, "Analysis of adhesive joints for aerospace applications," 2008.

[73] 3M, "Technical Datasheet - Structural Adhesive Film AF 191," pp. 1–12, 2009.

[74] 3M, "Technical Datasheet: Scotch-weld Structural Adhesive Film AF163-2," 2009.

[75] P. K. Sahoo, B. Dattaguru, and C. M. Manjunatha, "Strength Prediction of Adhesively Bonded Joints using Plastic Zone Size Criterion," *Procedia Eng.*, vol. 173, no. December, pp. 1635–1641, 2017.

[76] A. Fortunelli, C. Geloni, and A. Lazzeri, "Simulation of the plastic behavior of amorphous glassy bis-phenol-A- polycairbonate," *J. Chem. Phys.*, vol. 121, no. 10, pp. 4941–4950, 2004.

[77] P. N. B. Reis, L. Gorbatikh, J. Ivens, and S. V. Lomov, "Strain-rate sensitivity and stress relaxation of hybrid self-reinforced polypropylene composites under bending loads," *Compos. Struct.*, vol. 209, no. October 2018, pp. 802–810, 2019.

[78] M. Sepe, "Materials: Understanding Strain-Rate Sensitivity In Polymers," 2016. [Online]. Available: https://www.ptonline.com/articles/materials-understanding-

strain-rate-sensitivity-in-polymers. [Accessed: 02-Jun-2020].

[79] Y. M. Haddad and Y. M. Haddad, “Linear viscoelasticity,” *Viscoelasticity Eng. Mater.*, pp. 33–69, 1995.

[80] S. Turner, “Creep of Polymeric Materials,” *Encycl. Mater. Sci. Technol.*, pp. 1813–1817, 2001.

[81] P. N. B. Reis, M. P. Silva, and P. Santos, “Stress Relaxation in Delaminated Carbon/Epoxy Composites,” *Fibers Polym.*, vol. 20, no. 6, pp. 1284–1289, 2019.

[82] J. A. M. Ferreira, J. D. M. Costa, and P. N. B. Reis, “Static and fatigue behaviour of glass-fibre-reinforced polypropylene composites,” *Theor. Appl. Fract. Mech.*, vol. 31, no. 1, pp. 67–74, 1999.

[83] B. D. Davidson, M. Kumar, and M. A. Soffa, “Influence of mode ratio and hygrothermal condition on the delamination toughness of a thermoplastic particulate interlayered carbon/epoxy composite,” *Compos. Part A Appl. Sci. Manuf.*, vol. 40, no. 1, pp. 67–79, 2009.

[84] M. Raykyaguru, “Pros and Cons of Carbon Fiber,” *ResearchGate*, 2019.

[85] Y. Zhang, A. P. Vassilopoulos, and T. Keller, “Effects of low and high temperatures on tensile behavior of adhesively-bonded GFRP joints,” *Compos. Struct.*, vol. 92, no. 7, pp. 1631–1639, 2010.

[86] J. S. Earl, J. M. Dulieu-Barton, and R. A. Shenoi, “Determination of hygrothermal ageing effects in sandwich construction joints using thermoelastic stress analysis,” *Compos. Sci. Technol.*, vol. 63, no. 2, pp. 211–223, 2003.

[87] G. LaPlante and P. Lee-Sullivan, “Moisture effects on FM300 structural film adhesive: Stress relaxation, fracture toughness, and dynamic mechanical analysis,” *J. Appl. Polym. Sci.*, vol. 95, no. 5, pp. 1285–1294, 2005.